ARTICLES
https://doi.org/10.1038/s41590-018-0071-9
nature immunology

IL-17-receptor-associated adaptor Act1 directly stabilizes mRNAs to mediate IL-17 inflammatory signaling

Tomasz Herjan[1,2,9], Lingzi Hong[1,9], Jodi Bubenik[3], Katarzyna Bulek[1,4], Wen Qian[1], Caini Liu[1], Xiao Li[5], Xing Chen[1], Hui Yang[1], Suidong Ouyang[1], Hao Zhou[1], Junjie Zhao[1], Kommireddy Vasu[3], Eric Cockman[3], Mark Aronica[6], Kewal Asosingh[6], Donny D. Licatalosi[7], Jun Qin[8], Paul L. Fox[3], Thomas A. Hamilton[1], Donna Driscoll[3] and Xiaoxia Li[1*]

Mechanisms that degrade inflammatory mRNAs are well known; however, stabilizing mechanisms are poorly understood. Here, we show that Act1, an interleukin-17 (IL-17)-receptor-complex adaptor, binds and stabilizes mRNAs encoding key inflammatory proteins. The Act1 SEFIR domain binds a stem-loop structure, the SEFIR-binding element (SBE), in the 3′ untranslated region (UTR) of *Cxcl1* mRNA, encoding an inflammatory chemokine. mRNA-bound Act1 directs formation of three compartmentally distinct RNA–protein complexes (RNPs) that regulate three disparate events in inflammatory-mRNA metabolism: preventing mRNA decay in the nucleus, inhibiting mRNA decapping in P bodies and promoting translation. SBE RNA aptamers decreased IL-17-mediated mRNA stabilization in vitro, IL-17-induced skin inflammation and airway inflammation in a mouse asthma model, thus providing a therapeutic strategy for autoimmune diseases. These results reveal a network in which Act1 assembles RNPs on the 3′ UTRs of select mRNAs and consequently controls receptor-mediated mRNA stabilization and translation during inflammation.

IL-17, also known as IL-17A, is a key signature cytokine of type 17 helper T cells and is also produced by innate immune cells[1–3]. IL-17A plays a critical role in the pathogenesis of autoimmune and inflammatory diseases, including psoriasis, rheumatoid arthritis, multiple sclerosis and asthma[4–6].

IL-17A signals through a heterodimeric receptor complex (IL-17R) composed of IL-17RA and IL-17RC[7,8]. Both IL-17RA and IL-17RC belong to the SEFIR protein family, which is defined by the presence of a conserved cytoplasmic SEFIR domain[9]. Act1 (encoded by the gene *TRAF3IP2*, also known as *CIKS*) is an essential component in IL-17 signaling and is also a member of the SEFIR protein family[10–12]. After IL-17 stimulation, Act1 is recruited to IL-17R through a SEFIR-dependent interaction. Act1 in turn engages members of the TRAF family, activating the NF-κB, C/EBP and MAPK signaling pathways. IL-17–Act1-mediated signaling results in transcription of genes encoding proinflammatory and neutrophil-mobilizing cytokines and chemokines, including *Cxcl1*, *Tnf*, *Il6* and *Csf2* (ref. [13]).

Although IL-17 activates gene transcription of cytokines and chemokines, it is equally important for IL-17 to stabilize otherwise unstable mRNAs for the induction of expression of proinflammatory genes. Cytokine and chemokine mRNAs have short half-lives because of conserved cis elements, including AU-rich elements (AREs) and stem-loop structures in their 3′ UTRs[14,15]. The AREs within the 3′ UTRs can be recognized by RNA-binding proteins (including TTP, AUF1, KSRP and SF2) that mediate the sequential deadenylation, decapping and exonucleolytic degradation of RNA[16,17]. Stem-loops are present in immunologically related mRNAs (including *Tnf* and *Il6*) and are destabilized by the RNA-binding proteins Roquin and Regnase-1. Stress granules form in response to stress, store mRNAs stalled in translation and transfer them to processing (P) bodies for degradation. Roquin destabilizes translationally inactive mRNAs accumulated in P bodies and stress granules, whereas Regnase-1 specifically cleaves and degrades translationally active mRNAs bound to polysomes[18]. Although multiple mRNA-destabilizing mechanisms have been discovered, little is understood about the stabilization of mRNAs encoding inflammatory factors. Although the ARE-binding protein SF2 and human antigen R (HuR) have previously been implicated in IL-17-induced mRNA stabilization, the recruitment of SF2 and HuR cannot explain the receptor-specific mRNA stabilization of select inflammatory genes[19,20].

Here, we demonstrate that Act1 behaves as an RNA-binding protein that interacts with the stem-loop structure of select inflammatory mRNAs, such as *Cxcl1*, *Tnf* and *Csf2*. Act1 binding results in stabilization of the mRNA and thereby mediates the proinflammatory effects of IL-17 signaling. RNA aptamers containing the stem-loop structure (referred to herein as SBE) inhibited Act1's binding to target mRNAs, attenuated IL-17-mediated mRNA stabilization and ameliorated pathology in mouse models of asthma

[1]Department of Immunology, Lerner Research Institute, Cleveland Clinic Foundation, Cleveland, OH, USA. [2]Department of General Biochemistry, Faculty of Biochemistry, Biophysics and Biotechnology, Jagiellonian University, Krakow, Poland. [3]Department of Cellular and Molecular Medicine, Lerner Research Institute, Cleveland Clinic Foundation, Cleveland, OH, USA. [4]Department of Immunology, Faculty of Biochemistry, Biophysics, and Biotechnology, Jagiellonian University, Krakow, Poland. [5]Department of Genetics, Stanford University School of Medicine, Stanford, California, USA. [6]Department of Pathobiology, Lerner Research Institute, Cleveland Clinic, Cleveland, OH, USA. [7]Center for RNA Molecular Biology, Department of Biochemistry, Case Comprehensive Cancer Center, Case Western Reserve University, Cleveland, OH, USA. [8]Department of Molecular Cardiology, Lerner Research Institute, Cleveland Clinic Foundation, Cleveland, OH, USA. [9]These authors contributed equally: Tomasz Herjan and Lingzi Hong. *e-mail: lix@ccf.org

© 2018 Nature America Inc., part of Springer Nature. All rights reserved.

and skin inflammation. These data provide an initial example of a receptor-interacting adaptor molecule, Act1, playing a direct role in mRNA metabolism, and they elucidate a new mechanism of receptor-mediated selectivity of mRNA stabilization and translation. This mechanistic understanding of the action of Act1 might yield novel therapeutic strategies for treating inflammatory diseases.

Results

IL-17 induces distinct Act1 RNPs in the nucleus and cytoplasmic granules. mRNAs that are not engaged in translation can aggregate into cytoplasmic messenger RNP granules referred to as P bodies and stress granules[21,22]. IL-17A stimulation induced the assembly of Act1, the key adaptor of IL-17R, into microscopically visible cytoplasmic granules and nuclear localization (Fig. 1a and ref. [23]). Act1 colocalized with the decapping enzyme Dcp1, a component of P bodies (Fig. 1b), but not with TIA1 (a marker of stress granules) or the IL-1R-associated kinase IRAK1 (Fig. 1b). To investigate IL-17A-induced interaction of endogenous Act1 with Dcp1, we generated LSL–hemagglutinin tag (HA)–Act1 knock-in mice by knocking a LoxP-stop-LoxP-Traf3ip2 cDNA-HA-poly(A) cassette into the endogenous Act1 locus (Supplementary Fig. 1a and Methods). Using mouse embryonic fibroblasts (MEFs) isolated from UBC-Cre-ERT2/LSL-HA-Act1$^{f/+}$ mice, we detected the interaction between the endogenous HA-Act1 and Dcp1 in response to IL-17A stimulation by using in situ proximity ligation assays (Supplementary fig. 1b) and coimmunoprecipitation (Fig. 1c). RNase pretreatment of the lysates abolished the Act1–Dcp1 interaction (Fig. 1c), thus implicating a possible role of the IL-17–Act1 axis in mRNA metabolism in P bodies.

In addition to Act1–Dcp1 interaction, IL-17A induced interaction of HA-Act1 with SF2 and HuR in the nucleus and cytoplasmic granules, respectively (Supplementary Fig. 1c and ref. [20]). However, IL-17A stimulation did not induce visible interaction of Dcp1 with SF2 and HuR in either the nucleus or the cytoplasm (Supplementary Fig. 1c–f). These results indicated that Act1's interaction with Dcp1 in the P bodies was likely to be independent of the Act1–SF2 and Act1–HuR complexes. Notably, RNase pretreatment of the lysates abolished the Act1–SF2 and Act1–HuR interaction (Fig. 1c and Supplementary Fig. 1d–f). Together, these results implicate the IL-17–Act1 axis in mRNA metabolism via formation of distinct Act1-containing RNPs, including Act1–SF2 (RNP1), Act1–Dcp1 (RNP2) and Act1–HuR (RNP3). As a control, we showed that whereas IL-17E (also known as IL-25, another member of the IL-17 family) also induced the formation of Act1 RNPs (interaction with SF2, Dcp1 or HuR), IL-1 stimulation did not induce the formation of Act1 RNPs (interaction with SF2, Dcp1 or HuR) (data not shown).

The SEFIR domain of Act1 is required for the formation of Act1 RNPs. Deletion analysis showed that the SEIFR domain of Act1 was necessary and sufficient for Act1 assembly into granules and colocalization with Dcp1 (Fig. 1d and Supplementary Fig. 1g). Although SEFIR3 (residues 463–501) of Act1 is required for interaction with IL-17R[24], ΔSEFIR3 still localized to the P bodies (Fig. 1d and Supplementary Fig. 1g). Whereas ΔSEFIR5 showed decreased colocalization with P bodies, ΔSEFIR1 showed no localization to the P bodies (Fig. 1d and Supplementary Fig. 1g). ΔSEFIR1 also did not interact with Dcp1, SF2 and HuR in the coimmunoprecipitation experiment (Fig. 1e). However, both ΔSEFIR1 and ΔSEFIR5 retained their ability to interact with IL-17R (data not shown). Together, these results indicated that the SEFIR domain of Act1 is required for the formation of Act1 RNPs.

Act1 directly binds the *Cxcl1* 3′ UTR through the SEFIR domain. We then modeled the SEFIR domain of Act1 with SWISS-Model (http://swissmodel.expasy.org/), using the crystal structure of IL-17RA SEFIR as a template. Helix αA from SEFIR1 and helix αE from SEFIR5 are located in proximity in the Act1 SEFIR domain, forming a positively charged surface (Fig. 2a). The corresponding helix αA and helix αE from IL-17RA are not located on the same surface, and helix αE is negatively charged (Fig. 2a). We reasoned that the SEFIR1 and SEFIR5 positively charged surface in Act1 might provide an interaction interface with negatively charged mRNAs. To test this possibility, we subjected Act1 SEFIR and IL-17RA SEFIR to RNA electrophoretic mobility shift assays (REMSAs) on the *Cxcl1* 3′ UTR, which has been shown to be regulated by the IL-17–Act1 axis for stabilization of *Cxcl1* mRNA[25,26]. Recombinant Act1 SEFIR, but not IL-17RA SEFIR, bound to the *Cxcl1* probe with a dissociation constant (K_d) of 50.2 ± 7.8 nM (Fig. 2b and Supplementary Fig. 2a). Act1 SEFIR did not bind the GC-rich 3′ UTR of *Gpx4* mRNA (Fig. 2b). Whereas ΔSEFIR2, ΔSEFIR3 and ΔSEFIR4 retained the ability to bind RNA, ΔSEFIR1 and ΔSEFIR5 exhibited substantially lower binding to RNA (Supplementary Fig. 2b–f). Mutation of the positively charged amino acid residues in SEFIR1 (K407A) or SEFIR5 (K524A K526A K527A) substantially decreased the binding of Act1 SEFIR to RNA, whereas the K407A K524A K526A K527A mutant (SEFIR1 + 5mt) exhibited abolished RNA binding (Fig. 2c), thus supporting the proposed RNA-interaction interface of Act1 SEFIR in Fig. 2a. The impaired RNA binding of Act1 mutants (ΔSEFIR1 and SEFIR1 + 5mt) correlated with their inability to enter the P bodies (Fig. 1d and Supplementary Fig. 1g) and form RNPs (Fig. 1e and Supplementary Fig. 1d–f), a result consistent with the RNA-dependent interaction of Act1 with Dcp1, SF2 and HuR shown in Fig. 1c.

Act1 SEFIR binds a stem-loop structure in the *Cxcl1* 3′ UTR. In agreement with the observation that Act1 SEFIR bound nt 720–940 (*Cxcl1* 220, Figs. 2b and 3a), wild-type Act1, but not Act1 ΔSEFIR1 and ΔSEFIR mutants, stabilized reporter mRNA under the control of 3′ UTR-*Cxcl1* 220 in HeLa Tet-Off cells (Supplementary Fig. 4a). Act1 SEFIR bound nt 780–900 (*Cxcl1* 120) of the *Cxcl1* 3′ UTR with similar affinity (Fig. 3a,b). Secondary-structure prediction (RNAfold web server, http://rna.tbi.univie.ac.at/cgi-bin/RNAWebSuite/RNAfold.cgi/) indicated that nt 780–900 might form a secondary structure with four stem-loops (denoted A–D, Fig. 3b). We narrowed down the Act1-binding region to nt 810–857 (*Cxcl1* 47; Fig. 3a,b), an evolutionarily conserved region retaining stem-loops B and C (Fig. 3a), denoted the SBE (Fig. 3a,c). Binding of Act1 to the SBE was confirmed with surface plasmon resonance, which revealed a K_d of 59.5 nM (Supplementary Fig. 4b). Whereas disruption of stem-loop B did not affect Act1 SEFIR binding, impairment of stem-loop C completely prevented binding of Act1 SEFIR (Fig. 3c). Likewise, IL-17A stimulation did not attenuate *Cxcl1* mRNA decay in HeLa Tet-Off cells transfected with stem-loop C mutant (Fig. 3d). Together, the structure–function data suggested that Act1 SEFIR's binding to stem-loop C in the 3′ UTR of *Cxcl1* is required for IL-17A-induced *Cxcl1* mRNA stabilization.

To further map the Act1 SEFIR–binding site, we performed enzymatic RNA footprinting on the Act1 SEFIR–SBE complex. Nucleotides involved in the Act1–SBE interaction were identified through partial digestion of the SBE RNA, which was performed in the absence or presence of Act1 SEFIR. The native RNA and RNA–protein complexes were then partially digested with different RNases and analyzed by electrophoresis. The cleavage results with the native RNA (Fig. 3e) were consistent with the predicted structure shown in Fig. 3c. RNase A cleaves at single-stranded C and U bases (yellow in Fig. 3f). RNase T1 cleaves after single-stranded G bases (purple in Fig. 3f). RNase V1 cleaves in double-stranded regions (blue in Fig. 3f). Several nucleotides (U19, C31 and U33) were cleaved with both single-stranded and double-stranded nucleases, thus suggesting that these regions may 'breathe', which means that RNA nucleotides from this region may become transiently accesible. When the SBE was incubated with Act1 SEFIR, we observed partial protection of specific

© 2018 Nature America Inc., part of Springer Nature. All rights reserved.

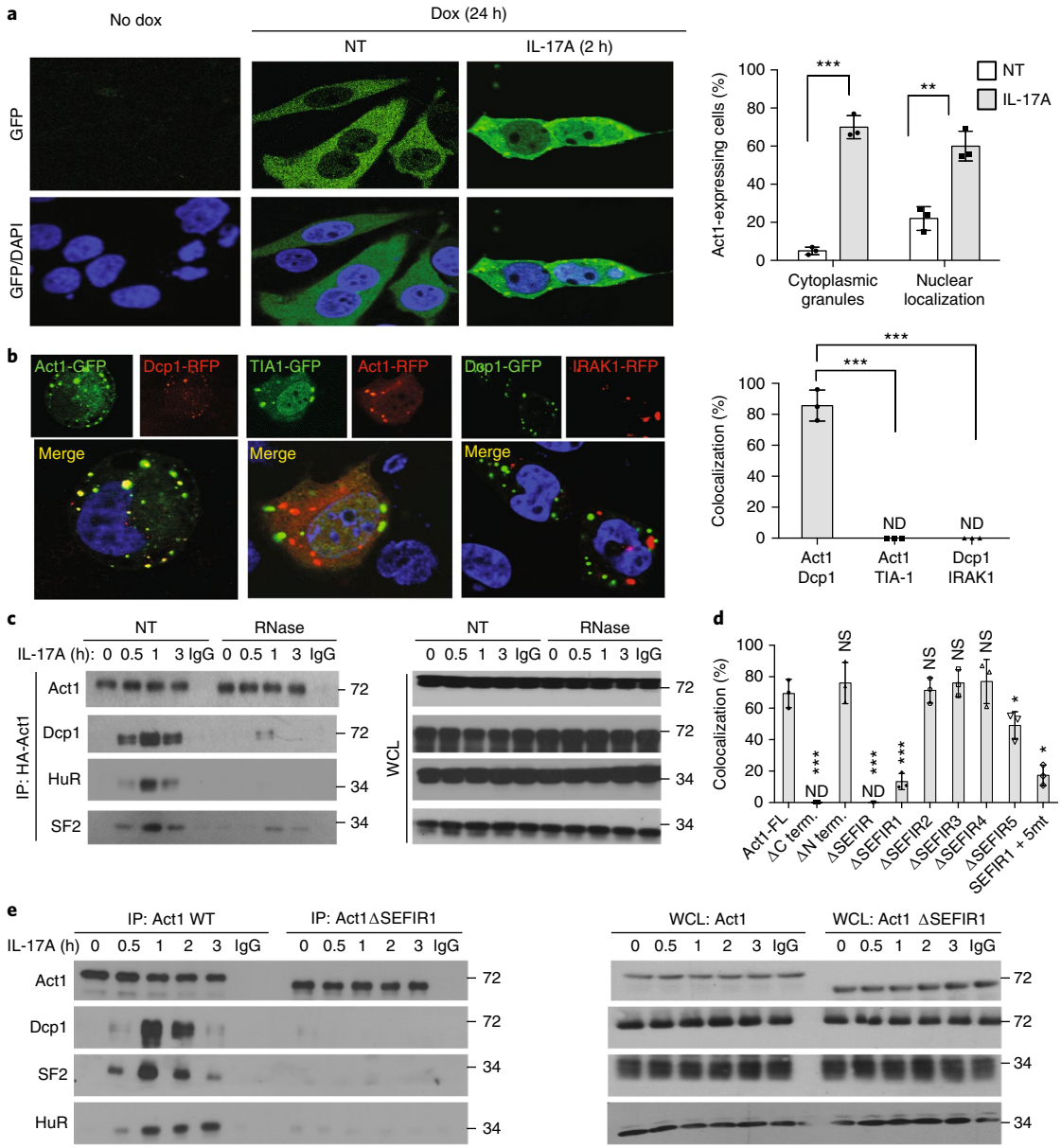


Fig. 1 | IL-17A induces distinct Act1 RNPs in the nucleus and cytoplasmic granules. a, Confocal imaging of Act1-GFP in a HeLa Tet-On stable cell line induced by doxycycline (dox) for 24 h, then stimulated with IL-17A or left untreated (NT). Blue, DAPI nuclear staining. Bar graph shows the mean and s.d. of percentages ($n = 3$ independent plates) of cells that display Act1 in the cytoplasmic granules or nuclear localization. 50 cells per plate were analyzed for quantification. **b**, Confocal imaging of HeLa cells cotransfected with GFP- or RPF-tagged expression constructs as indicated. Blue, DAPI nuclear staining. Bar graph shows the mean and s.d. of percentages ($n = 3$ independent plates) of cells with colocalization of the two expressing proteins (Act1/Dcp1, Act1/TIA1 and Dcp1/IRAK1). 50 cells per plate were analyzed for quantification. ND, not determined. **c**, Lysates from primary MEFs (isolated from LSL-HA-Act1 knock-in mice) stimulated with IL-17A (50 ng/ml), either left untreated or treated with RNase A, were immunoprecipitated (IP) with anti-HA (for endogenous HA-Act1), then subjected to western blot analysis with antibodies to the indicated proteins. WCL, whole cell lysate. The data are representative of three independent experiments. Throughout figure, numbers to the right of blots indicate molecular weight (kDa). **d**, Bar graph showing the mean and s.d. ($n = 3$ independent plates) of percentages of cells with colocalization of Dcp1 with full-length (FL) Act1 or Act1-deletion mutants (Supplementary Fig. 1g). Term, terminus. 50 expressing cells per plate were analyzed for quantification. **e**, *Act1*$^{-/-}$ MEFs reconstituted by retroviral infection with either FLAG-tagged mouse Act1 wild type (WT) or SEFIR1-deletion mutant were treated with IL-17A (50 ng/ml). The cell lysates were immunoprecipitated with anti-FLAG, then subjected to western blot analysis with antibodies to the indicated proteins. All data are representative of two independent experiments. *$P < 0.05$, **$P < 0.01$ and ***$P < 0.001$; NS, not significant. Scale bars, 20 μm.

nucleotides from cleavage by RNase A (U36 and U41–44) and RNase V1 (27–29, C31 and 36–40) (Fig. 3e). Minor protection between nucleotides 19 and 23 was occasionally observed, but the results were not consistent between experiments. Interestingly, bases U10–12 became more accessible to RNase A cleavage, thus suggesting that Act1 binding to stem-loop C may cause conformational changes in stem-loop B (bracket in Fig. 3e).

Together, the footprinting results validated that stem-loop C is the contact site for Act1 SEFIR. Disruption of the stem in stem-loop C (replacing CCC with GGG) abolished the binding of Act1 SEFIR to RNA, whereas replacement of the sequence in the stem of stem-loop C did not alter the binding of Act1 SEFIR, thus indicating that it is the secondary structure rather than the primary sequence that

© 2018 Nature America Inc., part of Springer Nature. All rights reserved.

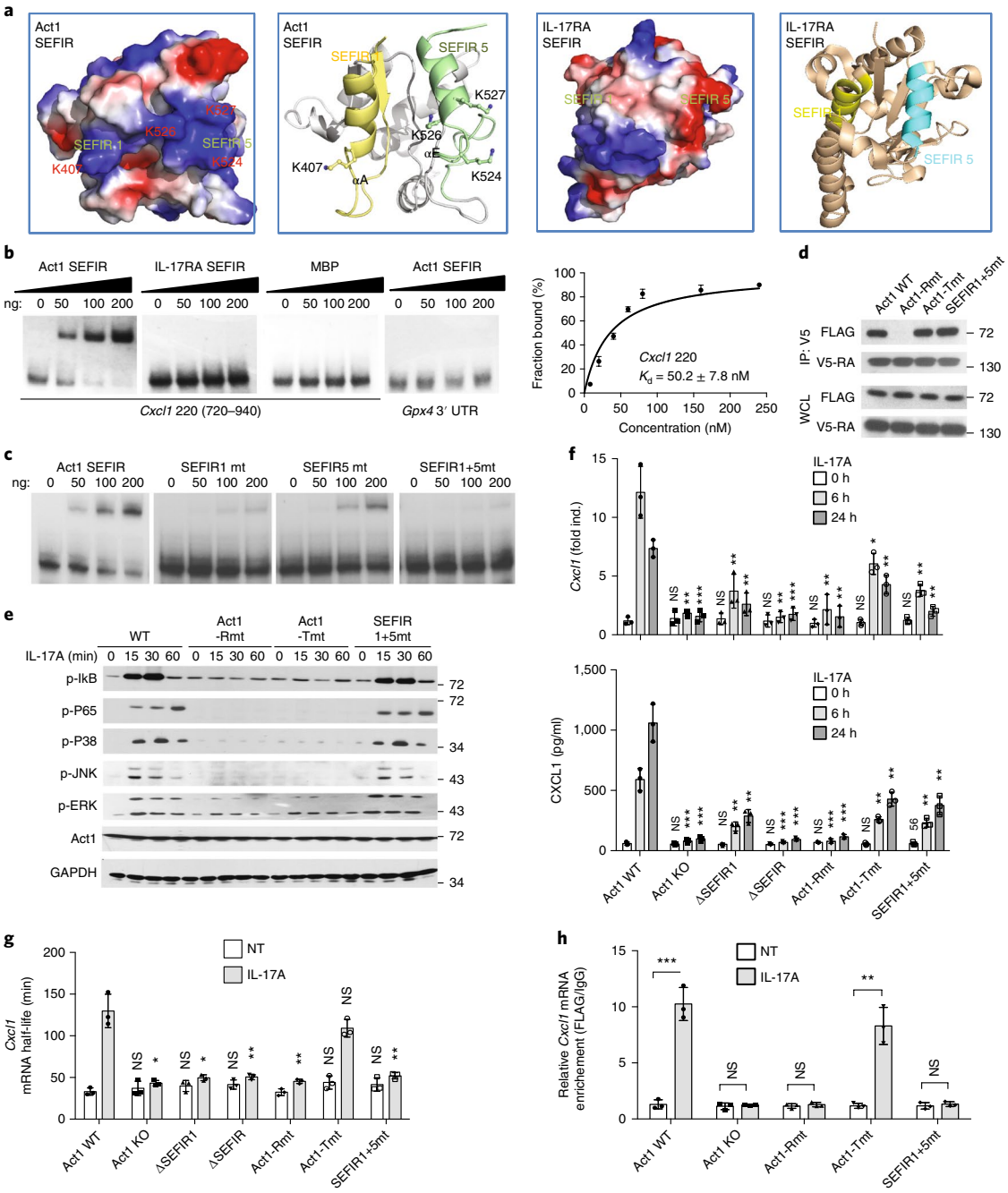


Fig. 2 | Act1 directly binds the CXCL1 3′ UTR through the SEFIR domain. a, Structural model of Act1 SEFIR. Blue and red, positive and negative electrostatic potential, respectively. **b**, Binding of purified recombinant Act1 SEFIR, IL-17RA SEFIR and histidine-tagged maltose-binding protein (MBP) to the *Cxcl1* 3′ UTR and *Gpx4* 3′ UTR, as determined by REMSA. Graph indicates the apparent K_d of the *Cxcl1* 3′ UTR (*Cxcl1* 220, as shown in Fig. 3a). Graph shows mean and s.d of three independent experiments. **c**, REMSA of purified recombinant Act1 SEFIR and SEFIR point mutants (mt) to the *Cxcl1* 3′ UTR (*Cxcl1* 220). **d**, FLAG-tagged Act1 WT and the indicated Act1 mutants were transfected into MEFs with V5-tagged IL-17RA. The cell lysates were immunoprecipitated with anti-V5, then subjected to western blot analyses with the indicated antibodies. Throughout figure, numbers to the right of blots indicate molecular weight (kDa). **e**, *Act1*$^{-/-}$ MEFs transfected with Act1 WT and Act1 mutants were treated with IL-17A for the indicated times. The cell lysates were analyzed by western blotting with antibodies to the indicated phosphorylated (p-) proteins. **f**, *Act1*$^{-/-}$ MEFs transfected with expression vectors for Act1 knockout (KO), Act1 WT or the indicated Act1 mutants were pretreated with TNF for 1 h and then either left untreated or stimulated with IL-17A. The mRNA and protein levels were analyzed by RT–PCR (top) and enzyme-linked immunosorbent assay (ELISA; bottom), respectively ($n = 3$ independent plates of cells). Ind, induction. **g**, *Act1*$^{-/-}$ MEFs transfected with expression vectors for Act1 KO, Act1 WT or the indicated Act1 mutants were pretreated with TNF for 1 h and then treated with actinomycin D either alone (NT) or in the presence of IL-17A for 25, 50, 70, and 100 min, then subjected to RT–PCR analysis ($n = 3$ independent plates of cells). The indicated mRNA levels were normalized to those of *Gapdh* and are presented as half-life. **h**. *Act1*$^{-/-}$ MEFs transfected with vector (Act1 KO), Flag-tagged Act1 WT or Act1 mutants were pretreated with TNF for 1 h, then treated with IL-17A for 0 and 60 min and subjected to anti-FLAG RNA immunoprecipitation and RT–PCR analyses of the indicated mRNAs ($n = 3$ independent plates of cells). Relative values to levels from IgG immunoprecipitation are shown. In **f**–**h**, bar graphs show mean and s.d. of independent plates of cells. *$P < 0.05$, **$P < 0.01$ and ***$P < 0.001$ (Act1 WT versus Act1 mutants or as indicated); NS, not significant. Data are representative of two (**c**–**h**) or three (**b**) independent experiments).

© 2018 Nature America Inc., part of Springer Nature. All rights reserved.

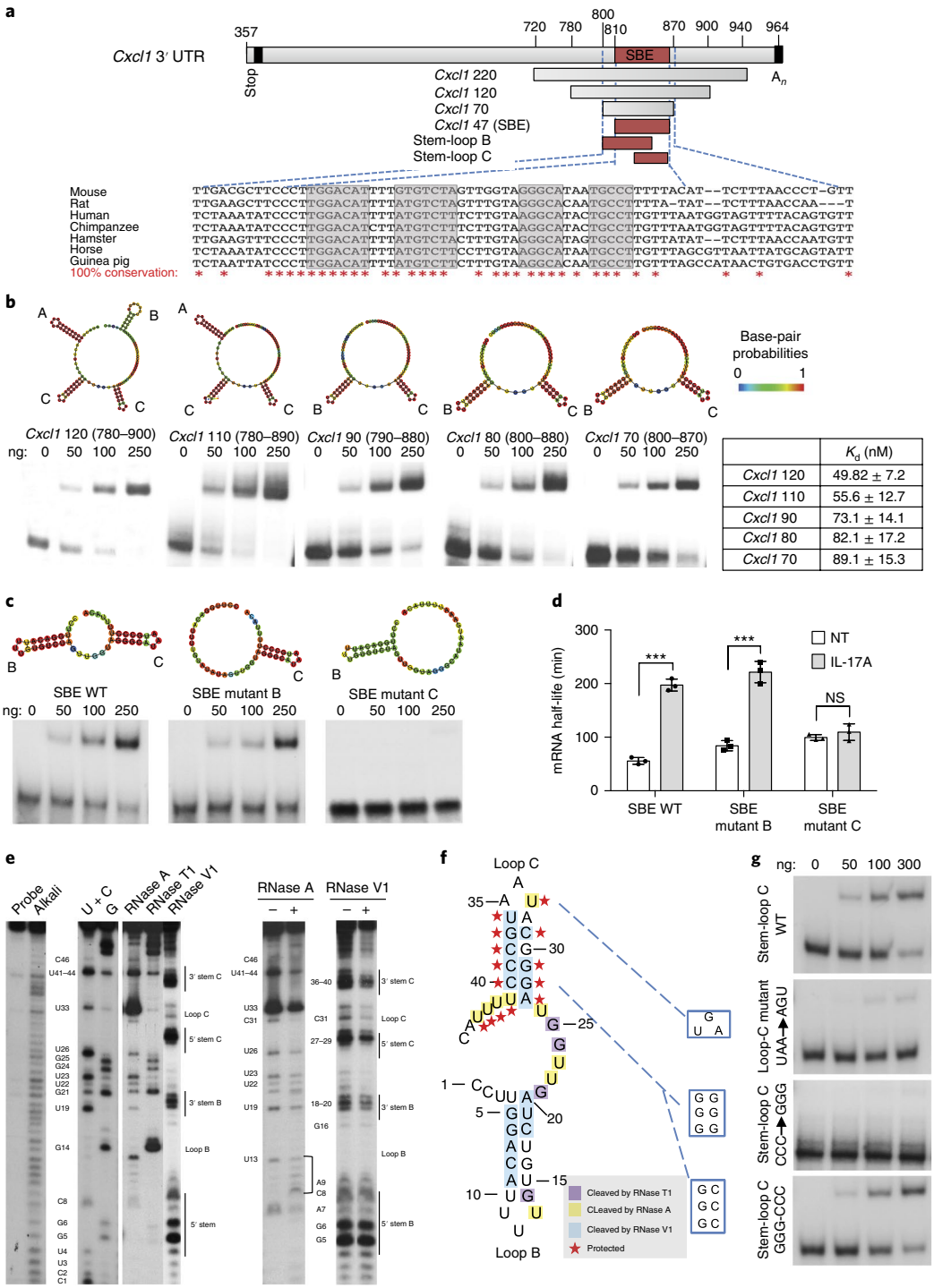


Fig. 3 | Act1 SEFIR binds a stem-loop structure in the *Cxcl1* 3′ UTR. a, Schematic representation of the mouse *Cxcl1* 3′ UTR together with an alignment of the region containing conserved stem-loops in the *Cxcl1* 3′ UTRs from the indicated species. Shaded boxes, conserved stem-loops. **b**, REMSA for the binding of purified recombinant Act1 SEFIR to the serial-deletion mutants from both ends of *Cxcl1* 220 (shown in **a**). Table shows the apparent K_d values (mean ± s.d.) of the serial-deletion mutants. **c**, Binding of purified recombinant Act1 SEFIR to SBE WT (*Cxcl1* 47, as indicated in **a**) and stem-loop B– and stem-loop C–disruption mutants. **d**, Real-time PCR analysis ($n = 3$ independent plates) of *Cxcl1* mRNA in HeLa Tet-Off cells transfected with pTRE2 (ref. [26]) with or without stem-loop B– or stem-loop C–disruption mutations, treated with doxycycline alone or together with IL-17A for 0, 45 or 90 min. *Cxcl1* mRNA levels were normalized to those of *Gapdh* and are presented as half-life. Bar graph shows mean and s.d. of independent plates of cells.*$P < 0.05$, **$P < 0.01$ and ***$P < 0.001$; NS, not significant. **e**, The 5′-end-labeled *Cxcl1* SBE was incubated in the absence or presence of Act1 SEFIR. The reactions were then partially digested with RNases T1, A or V1 as indicated. The sequencing (G and C + U) and alkali ladders are shown in the left lanes. The numbers to the left of the gels indicate the positions of nucleotides according to the numbering in **f**. The bands above C46 resulted from the remaining sequence in the plasmid template after restriction enzyme cutting. The different regions of the SBE are indicated. The red boxes indicate protected nucleotides in the SBE that were consistently observed. **f**, Structure of the SBE from the mouse *Cxcl1* mRNA. Asterisks indicate nucleotides protected from cleavage by RNase A and V1. **g**, Binding of purified recombinant Act1 SEFIR to the stem-loop C and mutants, as examined by REMSA. Data are representative of 2 (**c**) or 3 (**b**, **d**, **e** and **g**) independent experiments.

© 2018 Nature America Inc., part of Springer Nature. All rights reserved.

plays a critical role in Act1 SEFIR recognition (Fig. 3g). However, the replacement of the entire loop TAA of the stem-loop C with AGU (without affecting the formation of the stem-loop) also abolished SEFIR binding, thus demonstrating the importance of the loop sequence in Act1 SEFIR's RNA binding (Fig. 3g).

Act1 RNA binding to 3′ UTRs inhibits decapping. The next question that we sought to address was how Act1 RNA binding in Dcp1-containing P bodies mediates IL-17A-induced stabilization of otherwise unstable mRNAs of proinflammatory genes. mRNAs are decapped by the Dcp1 and Dcp2 decapping enzymes and then degraded 5′ to 3′ by the exonuclease Xrn1 (refs [28,29]). Because both coimmunoprecipitation and in situ proximity ligation assay showed that Act1 binds Dcp1, we examined whether Act1 binding to Dcp1 might affect the decapping activity of the Dcp1–Dcp2 complex. Purified Dcp1–Dcp2 and Act1 from transfected HeLa cells were incubated with the capped *Cxcl1* 3′ UTR (nt 720–940). There was indeed a dose-dependent inhibitory effect of Act1 (but not ΔSEFIR) on the decapping efficiency of the Dcp1–Dcp2 complex (Fig. 4a,b and Supplementary Fig. 5a). Additionally, Act1 did not protect the stem-loop C–disruption mutant transcript from decapping, thus confirming the importance of Act1 RNA binding in Act1's inhibition of decapping (Fig. 4a,b).

Act1 recruits TBK1, which disrupts the decapping complex via phosphorylation of Dcp1. IL-17A stimulation induced Dcp1 phosphorylation at S315 (Fig. 4c), which has been shown to be required for the inactivation of the decapping activity[30,31]. Although recent studies have reported two Act1-interacting kinases: IKKi and TBK1 (refs [32,33]) (Fig. 4d), IL-17A induced interaction of only TBK1 (not IKKi) with Dcp1 (Fig. 4c, Supplementary Fig. 1d–f and data not shown). IL-17A-induced Dcp1 phosphorylation (but not p65 phosphorylation) was diminished in TBK1-deficient cells, whereas IKKi deficiency had little effect (Supplementary Fig. 5b). Recombinant TBK1 phosphorylated Dcp1 in an in vitro kinase assay (Fig. 4e). TBK1 inhibitor blocked IL-17A-induced phosphorylation of TBK1–Dcp1 without affecting the interaction of TBK1 with Act1 or Dcp1, thus suggesting that TBK1 activation is not required for interaction with the Act1–Dcp1 complex (Fig. 4c). TBK1 overexpression diminished the interaction between Dcp1 and Dcp2, whereas TBK1 did not remove the Dcp1 S315A mutant from Dcp2 (Supplementary Fig. 5c). Furthermore, TBK1 inhibitor effectively abolished Act1-mediated inhibition of decapping (Fig. 4a.b), and immunodepletion of TBK1, but not IKKi, abolished Act1-mediated inhibition of decapping (Supplementary Fig. 5d,e). Moreover, TBK1 deficiency substantially decreased IL-17A-induced expression of *Cxcl1*, *Csf2* and *Tnf* at both the mRNA and protein levels (Fig. 4f). Together, these results suggest that Act1 may bring TBK1 to the mRNA targets in the P bodies, where TBK1 phosphorylates Dcp1, thereby resulting in Dcp1 dissociation from Act1 RNP, inhibition of decapping and stabilization of mRNAs.

Act1 forms distinct RNPs with Dcp1, Dcp2, SF2 and HuR. Our results defined an Act1 RNP consisting of Act1–TBK1–Dcp1–Dcp2, which we designated RNP2. Although imaging studies have indicated that SF2 and HuR do not colocalize with Dcp1 (Supplementary Fig. 1c), we performed immunoprecipitation experiments to examine the different Act1 RNPs. Whereas IL-17A induced Dcp1–Act1–TBK1 interaction in an RNA-dependent manner (sensitive to RNase treatment), SF2 and HuR were not detected in this RNP (RNP2) (Supplementary Fig. 1d). IL-17A-induced Act1–SF2 complex (RNP1) was also sensitive to RNase pretreatment, but Dcp1–TBK1 and HuR were not found in this Act1–SF2 RNP (Supplementary Fig. 1e). Likewise, we did not detect Dcp1–TBK1 and SF2 in IL-17A-induced Act1–HuR RNP (RNP3; Supplementary Fig. 1f). Together, these results suggest that Act1–SF2, Act1–Dcp1–Dcp2 and Act1–HuR represent three independent RNPs. Deletion of SEFIR1 (ΔSEFIR1) abolished the formation of all three RNPs, thus implicating the importance of Act1's binding to mRNA in the formation of these Act1 RNPs (Supplementary Fig. 1d–f).

SF2 has been shown to mediate decay of cytokine and chemokine mRNAs[34,35]. We have reported that SF2 binds chemokine mRNA (induced by TNF) in the absence of IL-17A stimulation[36]; however, the SF2–mRNA interaction substantially decreased after stimulation with IL-17A in an Act1-dependent manner (Fig. 5a and Supplementary Fig. 6a). Interestingly, we found that IL-17A did not decrease SF2's binding to *Cxcl1* in Act1-deficient cells restored with ΔSEFIR1, thus suggesting that Act1's RNA binding might be required for the dissociation of SF2 from the mRNAs (Fig. 5a). One important question is how Act1's binding to mRNAs promotes the dissociation of SF2 from mRNAs. We found that SF2 bound the same region on *Cxcl1* as Act1, the SBE, and that the impairment of stem-loop C completely prevented the binding of SF2 (Fig. 5b and Supplementary Fig. 6b). Addition of increasing amounts of Act1 to the RNA binding reaction attenuated SF2's binding to the SBE (Fig. 5c). Notably, SF2 phosphorylation has been implicated as a mechanism for its dissociation from mRNA targets[37]. Although both imaging and fractionation experiments indicated that Act1–SF2 RNP1 resides in the nucleus (Supplementary Figs. 1c and 6c), IKKi, a kinase required for IL-17A-mediated mRNA stabilization[32], translocated into the nucleus and was detected in Act1–SF2 RNP1 in response to IL-17A stimulation (Supplementary Fig. 6c). IKKi indeed was able to phosphorylate SF2 in vitro (Fig. 5d), and incubation of recombinant IKKi with SF2 decreased the ability of SF2 to bind *Cxcl1* mRNA (Supplementary Fig. 6d), thus implicating IKKi in preventing SF2's binding to mRNAs. Whereas IL-17A-induced IKKi–SF2 and Act1–SF2 interaction were abolished in Act1-deficient MEFs restored with ΔSEFIR1 (Fig. 5a and Supplementary Fig. 6c), Act1–IKKi interaction in both the cytosol and nucleus was retained in these cells (Supplementary Fig. 6c). These results suggested that IL-17A induces Act1–IKKi interaction before their translocation to the nucleus, and Act1's binding to SF2-bound mRNAs in the nucleus allows IKKi to phosphorylate SF2, thereby attenuating SF2's binding to the mRNA targets.

HuR has been implicated in shifting target mRNAs to polysomes for protein translation, and IL-17A stimulation induces the coshift of Act1–HuR to the polysomes[20,38]. IL-17A induced the binding of HuR to *Cxcl1* in Act1-expressing MEFs, and this effect was abolished in Act1-deficient MEFs restored with ΔSEFIR1, thus suggesting that Act1's RNA binding might also be required for HuR's recruitment to the target mRNAs (Fig. 5a). We found that HuR bound CXC1 220-I but not CXC1 220-II (Fig. 5b and Supplementary Fig. 6e). HuR and Act1 were found to simultaneously bind CXC1 220 (Fig. 5e). Removal of nt 720–829 from CXC1 220 abolished HuR binding, whereas Act1 binding was retained, thus indicating that HuR and Act1 have independent binding sequences on *Cxcl1* (Fig. 5b,e). Because HuR is not part of RNP1 (Act1–SF2) (Supplementary Fig. 1c–f), Act1 may facilitate HuR's binding to *Cxcl1* in vivo after competing SF2 away from target mRNAs. In support of this possibility, the IL-17A-induced coshift of Act1–HuR to the polysomes[20] was abolished in Act1-deficient MEFs restored with ΔSEFIR1 (Fig. 5f-g). The ratio of *Cxcl1* mRNA in translation-active polysomes over the inactive fractions substantially decreased in Act1-deficient MEFs restored with ΔSEFIR1 (Fig. 5g,h). On the basis of these results, we propose the following model for the actions of Act1 RNA binding (Supplementary Fig. 1h). First, IL-17 induces Act1's binding to mRNAs (such as *Cxcl1*) in the nucleus (RNP1), thereby preventing SF2-mdiated mRNA decay by competing away SF2's binding to the mRNAs, an effect further promoted by IKKi-mediated SF2 phosphorylation. Second, Act1 follows the mRNAs to the P bodies (RNP2) and subsequently inhibits Dcp1–Dcp2-mediated

© 2018 Nature America Inc., part of Springer Nature. All rights reserved.

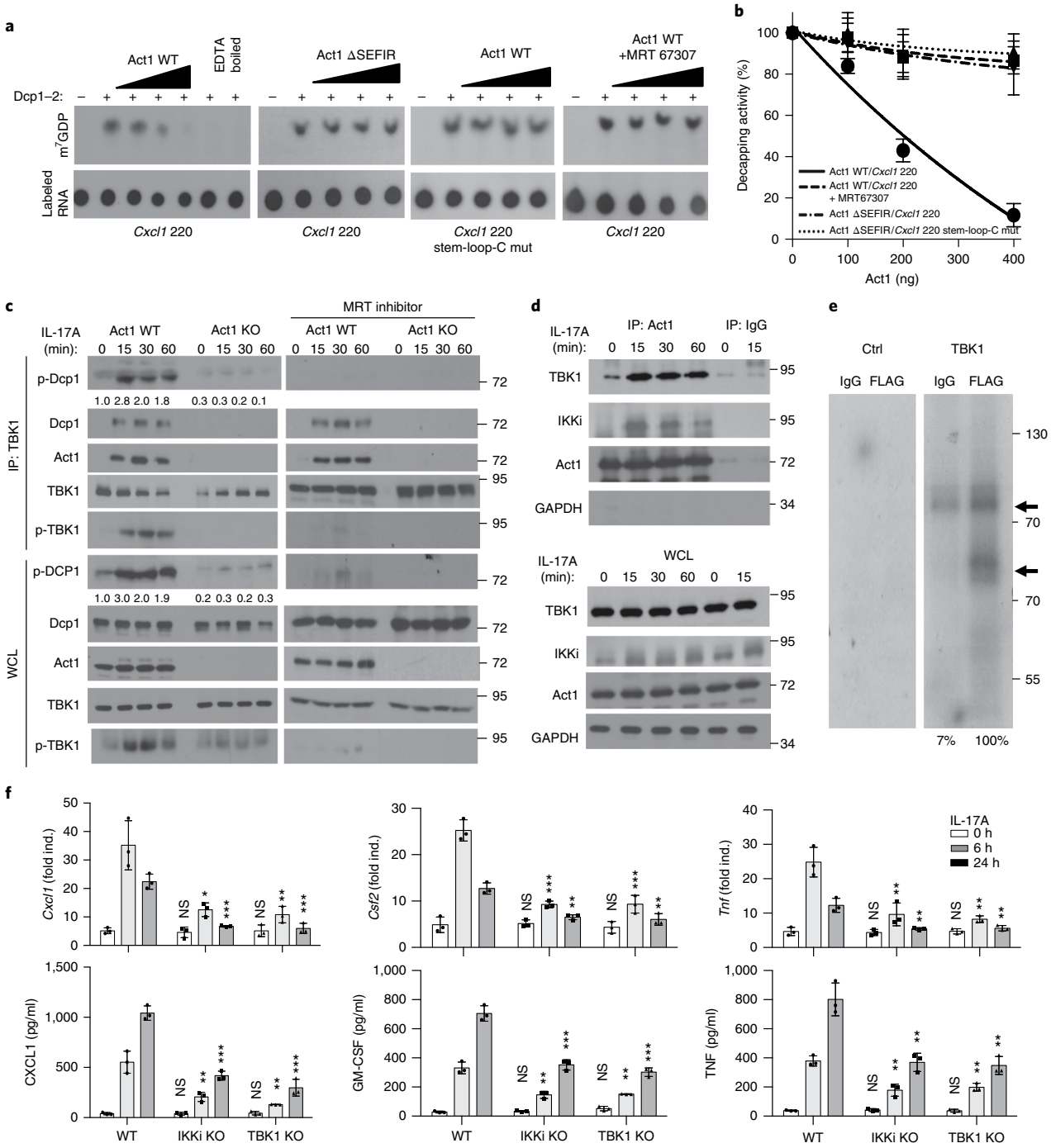


Fig. 4 | Act1 RNA binding to the 3′ UTR inhibits decapping through TBK1-mediated phosphorylation of Dcp1. a, Cap (m^7GDP)-labeled reporter RNAs (Cxcl 220 and mutant (mut) without stem-loop C (Cxcl 220 stem-loop C mutant)) were subjected to decapping assays with purified Dcp1–Dcp2 with increasing amounts of purified Act1 WT or Act1 ΔSEFIR in the presence or absence of TBK1 inhibitor (MRT67307). EDTA and boiling were included as negative controls to inactivate Dcp1–Dcp2 enzymatic activity. Radiograms were quantified by densitometry. **b**, Decapping activity calculated by quantifying the released cap as a percentage of the amount of cap catalyzed by purified Dcp1–Dcp2. Error bars represent mean and s.d. of three independent experiments. **c**, Cell lysates from *Act1*$^{-/-}$ MEFs, with or without reconstitution with Act1 WT or Act1 KO, and in the presence or absence of TBK1 inhibitor (MRT67307), were immunoprecipitated with anti-TBK1, then subjected to western blot analysis with antibodies to the indicated proteins. Throughout figure, numbers to the right of blots indicate molecular weight (kDa). **d**, Cell lysates from untreated and IL-17A-treated HeLa cells were immunoprecipitated with anti-Act1, then subjected to western blot analysis with antibodies to the indicated proteins. **e**, In vitro kinase assay of Dcp1 with or without (Ctrl) recombinant TBK1, using Dcp1 immunoprecipitates from HeLa cells transfected with FLAG-tagged Dcp1. **f**, WT, IKKi-deficient (IKKi KO) and TBK1-deficient (TBK1 KO) MEFs were pretreated with TNF for 1 h, then left untreated or stimulated with IL-17A. The mRNA and protein levels were then analyzed by RT–PCR (top) and ELISA (bottom), respectively (n = 3 independent plates of cells). Bar graphs show mean and s.d. of independent plates of cells. *P < 0.05, **P < 0.01 and ***P < 0.001 (WT versus KO); NS, not significant. Data are representative of two (**c**, **d**, **f**) or three (**a**, **e**) independent experiments.

© 2018 Nature America Inc., part of Springer Nature. All rights reserved.

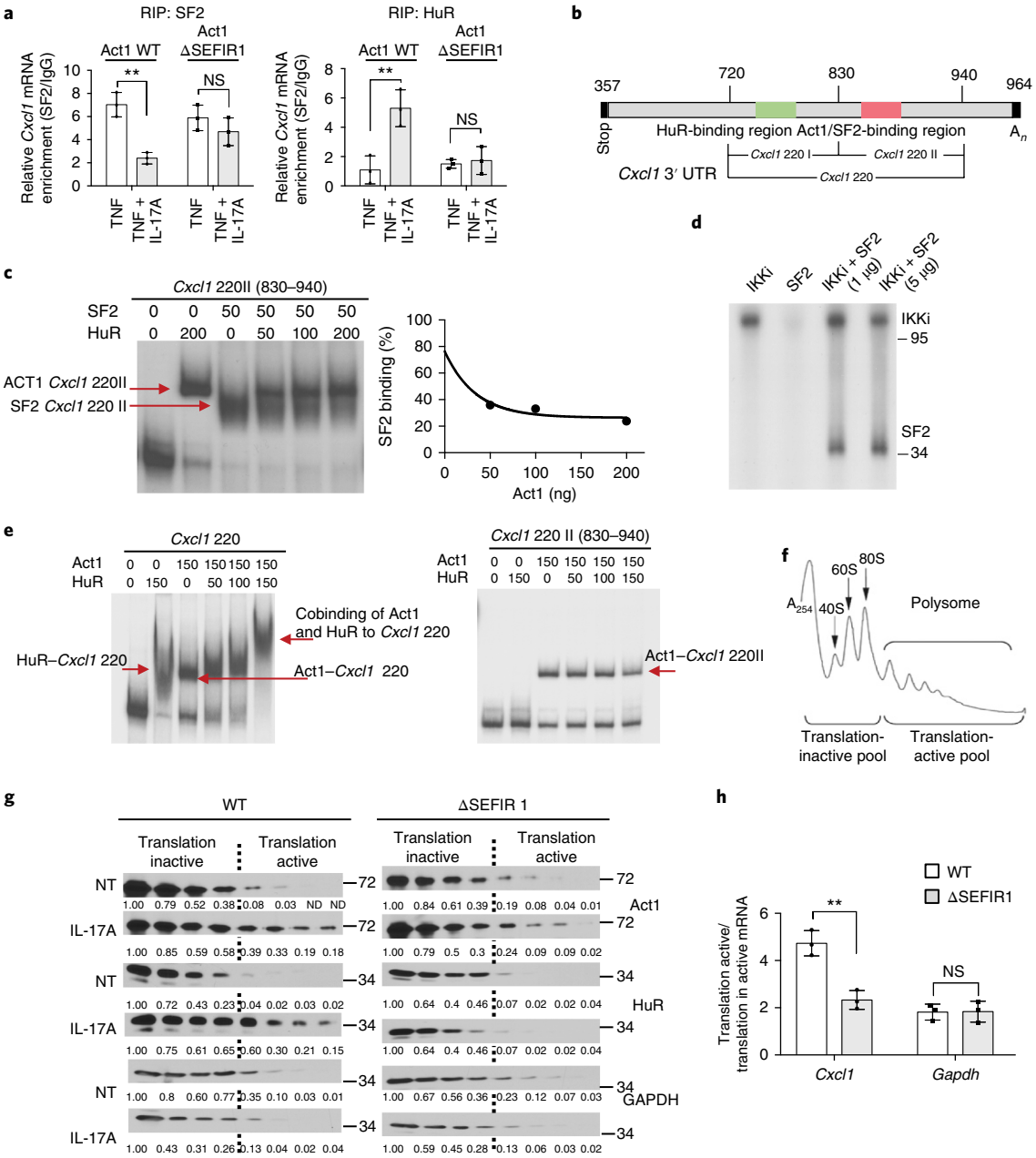


Fig. 5 | Act1 forms distinct RNPs with Dcp1, Dcp2, SF2 and HuR. a, *Act1*$^{-/-}$ MEFs reconstituted by retroviral infection with either Act1 WT or ΔSEFIR1 were pretreated with TNF for 1h, then treated with IL-17A for 0 or 60 min and subjected to RNA immunoprecipitation with anti-SF2 or anti-HuR, and RT–PCR analyses ($n = 3$ independent plates of cells) of the indicated mRNAs. Relative values normalized against IgG control are shown. **b**, Schematic representation of the mouse *Cxcl1* 3′ UTR. HuR-, Act1- and SF2-binding regions are indicated. **c**, Act1 SEFIR and SF2 RNA binding competition, performed with probe *Cxcl1* 220 II (as indicated in **b**). Graph indicates the dissociation of SF2-*Cxcl1* 220 II after incubation with increasing amounts of Act1 SEFIR, which was calculated by quantifying the remaining SF2–*Cxcl1* 220 II complex in the presence of indicated amounts of Act1 SEFIR. **d**, In vitro kinase assay of purified recombinant IKKi, using purified recombinant SF2 as a substrate. Numbers to right of gel indicate molecular weight (kDa). **e**, Simultaneous binding of purified recombinant HuR and Act1 SEFIR to the *Cxcl1* 3′ UTR, examined by REMSA with *Cxcl1* 220 and *Cxcl1* 220 II as probes. Cobinding of Act1 and HuR was observed with probe *Cxcl1* 220, but not *Cxcl1* 220 II. **f**, UV-absorbance profile of RNP and polysome complexes separated on a sucrose density gradient into different fractions, as indicated. **g**, Cytoplasmic extracts of *Act1*$^{-/-}$ MEFs reconstituted by retroviral infection with either FLAG-tagged mouse Act1 WT or SEFIR1-deletion mutant, pretreated with TNF for 1h and then treated with IL-17A for 0 or 90 min, were fractionated through a 10–50% sucrose gradient and analyzed by western blot analyses with antibodies to the indicated proteins. Numbers to right of blots indicate molecular weight (kDa). **h**, *Cxcl1* mRNAs from translation-active pools and translation-inactive pools from **f** were analyzed by RT–PCR and normalized to β-actin. Graph shows the ratios of mRNAs from translation-active/inactive pools ($n = 3$ independent plates of cells). All data are representative of three independent experiments. Bar graphs in **a** and **h** show mean and s.d. of independent plates of cells. $^{**}P < 0.01$ and $^{***}P < 0.001$; NS, not significant.

mRNA decapping by using TBK1 to phosphorylate Dcp1. Finally, Act1 mRNAs are shifted to the polysomes by facilitating HuR's binding to mRNAs (RNP3) for protein translation.

SBE RNA aptamers abolished IL-17A-induced mRNA stabilization of *Cxcl1*, *Csf2* and *Tnf*. We then hypothesized that RNA oligonucleotides corresponding to the SBE might inhibit the effects

© 2018 Nature America Inc., part of Springer Nature. All rights reserved.

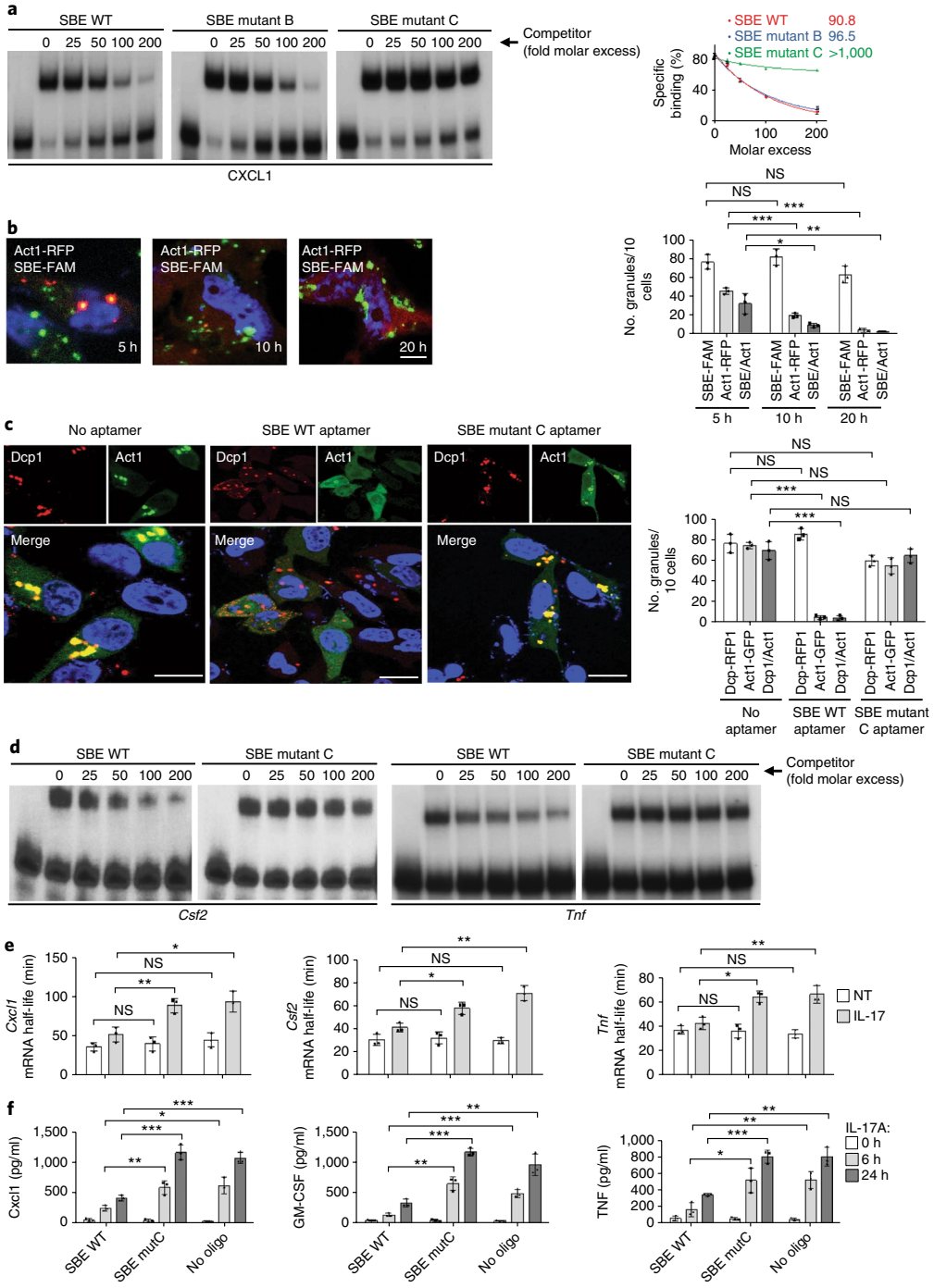


Fig. 6 | SBE RNA aptamers abolished IL-17A-induced mRNA stabilization of *Cxcl1*, *Csf2* and *Tnf*. a, SBE RNA aptamers (SBE WT (*Cxcl1* 47), SBE mutant B and SBE mutant C) were used to compete with *Cxcl1* 220 probe for binding to Act1 SEFIR. Graph quantifies the remaining Act1 SEFIR-bound *Cxcl1* 220 probe in the presence of the indicated concentrations of SBE aptamers. **b**, Confocal imaging of RFP-Act1 and fluorescein amidite–labeled SBE aptamer (SBE-FAM) in transfected HeLa cells. Blue, DAPI nuclear staining. Graph indicates the average numbers and s.d. ($n = 3$ independent plates of cells) of SBE-FAM-positive, Act1-RFP-positive and SBE-FAM/Act1-RFP-double-positive granules per ten cells at 5, 10 and 20 h after SBE-FAM transfection. 50 cells per plate were analyzed for quantification. **c**. Confocal imaging of Dcp1-RFP- and Act1-GFP-expressing HeLa cells transfected with 100 pmol/ml of unlabeled SBE aptamers. Blue, DAPI nuclear staining. Graph indicates the average numbers and s.d. ($n = 3$ independent plates of cells) of Dcp1-RFP-positive, Act1-GFP-positive and Dcp1-RFP/Act1-GFP-double-positive granules per ten cells 24 h after SBE-FAM transfection. 50 cells per plate were analyzed for quantification. **d**, SBE RNA aptamers (SBE WT (*Cxcl1* 47) and SBE mutant C) were used to compete with GM-CSF 3′ UTR (513–785) and TNF 3′ UTR (1362–1507) probes for binding to Act1 SEFIR. **e**, RNA decay in HeLa cells transfected with 100 pmol/ml of SBE RNA aptamers (WT or mutant C) or no oligonucleotide (no oligo), pretreated with TNF for 1 h and then treated with actinomycin D alone (NT) or in the presence of IL-17A for 45 or 90 min. Human *Cxcl1*, *Csf2* and *Tnf* mRNAs were measured by RT–PCR ($n = 3$ independent plates of cells), normalized to *Gapdh* and presented as half-life. **f**, HeLa cells transfected with 100 pmol/ml of SBE RNA aptamers (WT or mutant C) or no oligonucleotide, pretreated with TNF (10 ng/ml) for 1 h and then subjected to stimulation with IL-17A for 0, 6 or 24 h. Supernatants of the treated cells were then analyzed by ELISA. Data are representative of two (**a**, **d**) or three (**b**, **c**, **e** and **f**) independent experiments. Bar graph shows mean and s.d. of independent plates of cells. $^*P < 0.05$, $^{**}P < 0.01$ and $^{***}P < 0.001$; NS, not significant. Scale bars, 20 μm.

© 2018 Nature America Inc., part of Springer Nature. All rights reserved.

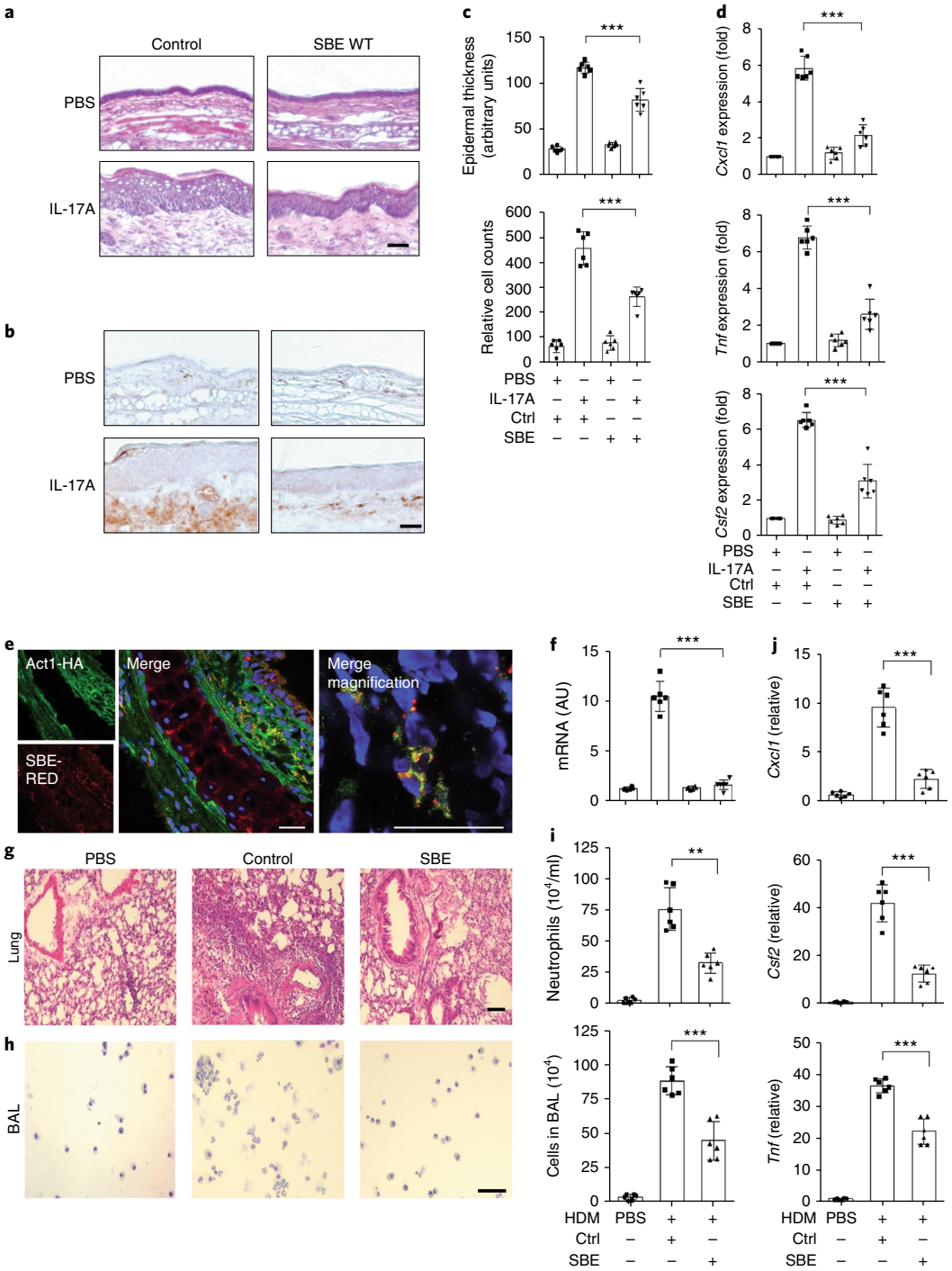


Fig. 7 | SBE RNA aptamers inhibited IL-17A-dependent skin hyperplasia and HDM-induced airway inflammation. a, Hematoxylin–eosin staining of ear skin tissue from C57BL/6 J mice ($n = 6$ mice/group) injected intradermally with IL-17A (500 ng) or PBS together with 1 nmol of methylated SBE mutant C (Control or Ctrl) or SBE WT aptamer for six consecutive days. **b**, Paraffin sections of the ear skin from mice in **a** were subjected to immunohistochemistry staining for Ly6G. **c**, Epidermal thickness of ear skin from mice in **a** were measured in arbitrary units, and the average number of Ly6G$^+$ cells per section from **b** was counted. Five fields were analyzed for each mouse under 20× magnification. Bar graphs show mean ± s.e.m. of biological replicates. **d**, RT–PCR analysis of mRNA isolated from the ear skin tissue from mice in **a**. Expression of Act1-target genes is graphed as mean fold induction over the PBS + control aptamer–treated group. Data represent mean ± s.e.m. of biological replicates ($n = 6$ mice/per group). **e**, Confocal imaging of tracheas from HA-Act1 knock-in mice treated with methylated, fluorescently labeled SBE WT aptamers (red) and anti-HA stained (green). Images were acquired at 40× magnification and 63× magnification. Blue, DAPI nuclear staining. **f**, Relative abundance of IL-17A and IL-17E isolated from lung tissue, determined by RT–PCR analysis ($n = 6$ mice/group). **g**,**h**, C57BL/6 J mice were sensitized and challenged with HDM, then subjected to treatment with methylated SBE mutant C (Control or Ctrl) or SBE WT aptamer ($n = 6$ mice/group). Lung tissue (**g**) and BAL (**h**) were subjected to paraffin sectioning and cytospins, then hematoxylin–eosin and HEMA3 staining respectively. **i**, Total and neutrophil cell numbers in the BAL of the indicated mice ($n = 6$ mice/group) were manually counted. **j**, RT–PCR analysis of Act1-target genes in the lung tissues from mice ($n = 6$ mice/group) treated as in **e**. Graphs show mean fold induction over PBS + control aptamer–treated group. Throughout figure, data represent mean ± s.e.m. of biological replicates. $^*P < 0.05$, $^{**}P < 0.01$ and $^{***}P < 0.001$; NS, not significant. All data are representative of three independent experiments. Scale bars, 100 μm.

© 2018 Nature America Inc., part of Springer Nature. All rights reserved.

of Act1 in the defined RNPs and in inflammatory gene expression. SBE RNA aptamer and mutant stem-loop B aptamer (but not mutant stem-loop C) were able to compete away Act1 SEFIR's binding to the *Cxcl1* 3′ UTR (Fig. 6a). The transfected fluorescent SBE RNA aptamers mainly resided in the cytoplasm and were detected in Act1 granules (Fig. 7b and Supplementary Fig. 6a). Act1 granules substantially decreased over time in cells transfected with SBE RNA aptamers, thus suggesting that the SBE RNA aptamers might be disrupting Act1's colocalization with P bodies (Fig. 6c). SBE RNA aptamers, but not SBE aptamers with mutated stem-loop C, abolished the formation of Act1 granules and Act1's colocalization with Dcp1 (Fig. 6c). Furthermore, SBE RNA aptamers specifically disrupted endogenous Act1–Dcp1 and Act1–HuR interaction in the cytoplasm but had no effect on Act1–SF2 interaction in the nucleus (Supplementary Fig. 7b), a result consistent with the observation that SBE RNA aptamers mainly resided in the cytoplasm (Fig. 6b and Supplementary Fig. 7a). SBE RNA aptamers were also able to compete away Act1 SEFIR binding to the 3′ UTRs of *Csf2* and *Tnf* mRNAs (Fig. 6d and Supplementary Fig. 7c), thus suggesting that the binding of SBE RNA aptamers to Act1 SEFIR blocks Act1's binding to the mRNA targets. These results suggest that the SBE RNA aptamers have the potential to be an inhibitory agent for blocking the IL-17A-induced inflammatory response. We indeed found that transfection of SBE RNA aptamers decreased IL-17A- and IL-17E-mediated, but not IL-1-mediated, mRNA stabilization and the production of the chemokine CXCL1 and the cytokines GM-CSF and TNF (Fig. 6e,f and Supplementary Fig. 7d–g).

SBE RNA aptamers inhibited IL-17A-dependent skin and lung inflammation. Secukinumab (anti-IL-17A) has shown great efficacy in psoriasis treatment and has been approved by the US Food and Drug Administration for this application. Aberrant keratinocyte proliferation and neutrophilic inflammation are well-known hallmarks of the pathogenesis of psoriasis. We found that the SBE RNA aptamer, but not mutant aptamer, substantially decreased IL-17A-dependent epidermal hyperplasia and neutrophil infiltration in the ears (Fig. 7a–c). Likewise, SBE RNA aptamer, but not mutant aptamer, greatly diminished IL-17A-induced expression of *Cxcl1*, *Csf2* and *Tnf* in the ears (Fig. 7d). Together, these data indicate that IL-17A induced keratinocyte proliferation and neutrophil infiltration, thus resulting in epidermal hyperplasia, and these effects were blocked by SBE RNA aptamers.

House dust mites (HDM), a natural allergen to which people with asthma are often sensitized, can induce neutrophilic airway inflammation, which is often associated with severe asthma[39]. In agreement with reports from the literature, we found that IL-17RC-knockout (but not IL-17RB-knockout) mice, compared with wild type, showed substantially less neutrophilic airway inflammation in a severe asthma model induced by high-dose HDM (ref. [40] and data not shown), during which IL-17 (but not IL-17E) was highly induced (Fig. 7f). Tracheal section of mice subjected to intranasal administration of fluorescently labeled SBE RNA aptamers showed efficient tissue penetration of SBE RNA aptamers (Fig. 7e) and their colocalization with Act1 inside the cells (Fig. 7e). We then evaluated the ability of SBE RNA aptamers to alleviate neutrophilia in this IL-17A-dependent severe asthma model. HDM-induced neutrophilia and inflammatory gene expression in bronchoalveolar lavage (BAL) and lung tissue were substantially decreased by treatment with SBE RNA aptamers (Fig. 7g–j). Together, the results from HDM experiments indicate a potential therapeutic role of SBE RNA aptamers in treatment of IL-17A-mediated severe asthma.

Discussion

The SEFIR domain, a conserved motif present in the cytoplasmic regions of IL-17R subunits and the adaptor Act1, mediates the recruitment of Act1 to the receptor after IL-17 stimulation. Here, we unexpectedly identified SEFIR of Act1 as a direct RNA-binding domain that allows Act1 to bind and stabilize otherwise unstable mRNAs of proinflammatory genes (*Cxcl1*, *Csf2* and *Tnf*) in response to IL-17 stimulation. Act1 directly binds the 3′ UTRs of inflammatory mRNAs and forms distinct RNPs in several subcellular compartments, including P bodies, controlling mRNA metabolism. Structure–function analysis showed that Act1 SEFIR binds a stem-loop structure (termed the SBE) in the *Cxcl1* 3′ UTR. RNA aptamers containing the SBE abolished Act1's binding to the target mRNAs and attenuated IL-17-mediated mRNA stabilization. Furthermore, SBE RNA aptamers inhibited IL-17A-induced skin inflammation and decreased airway inflammation in an HDM-induced asthma model. Together, our results demonstrate that the receptor-proximal adaptor Act1 directly binds mRNAs and controls the steps of RNA metabolism, thus providing a novel molecular mechanism of inflammatory response via the receptor-specific mRNA stabilization of select inflammatory genes. Moreover, the discovery of a noncanonical function of Act1 should allow for the development of new therapeutic strategies for autoimmune inflammatory diseases.

We and others have previously shown that Act1 is required for IL-17R-mediated signaling including that of NF-κB, JNK, p38 and ERK[13]. The Act1 mutants defective in RNA binding retained the ability to interact with IL-17RA and were able to mediate IL-17-induced NF-κB, JNK, ERK and p38 activation. These data indicate a novel function of Act1 as an RNA-binding protein for mRNA stabilization, which is separate from its role as an adaptor. Using Act1 mutants defective in binding to the receptor or TRAF6, we found that the recruitment of Act1 to IL-17RA is required for IL-17-induced Act1 RNA binding in the cells, whereas Act1 binding to TRAF6 (and its ability to activate NF-κB) is independent of Act1's RNA binding activity. This study intriguingly reveals the selective recruitment of IKKi to Act1 RNP1 (SF2 complex) and TBK1 to Act1 RNP2 (Dcp1 complex). Additionally, TBK1, but not IKKi, was required for IL-17-induced Dcp1 phosphorylation. Recent studies have implied that distinct scaffold proteins assemble TBK1 and IKKi subcomplexes, in a stimulus-specific manner, thus potentially representing a mechanism to achieve specificity[41–44].

We propose the following model for the actions of Act1 RNA binding in the IL-17-induced inflammatory response. After IL-17 stimulation, multiple signaling pathways (including the NF-κB and MAPK pathways) are activated to induce the gene transcription of cytokines and chemokines. Act1 then directly binds the mRNAs of cytokines and chemokines and consequently stabilizes these otherwise unstable mRNAs for the production of the proinflammatory mediators. Act1's binding to mRNAs of inflammatory genes results in the formation of multiple RNPs controlling different steps of mRNA metabolism. The present study provides an initial example of a receptor-interacting adaptor molecule, Act1, playing a direct role in mRNA metabolism and orchestrating receptor-mediated selectivity of mRNA stabilization and translation. Considering the efficacy of SBE RNA aptamers in blocking IL-17-dependent skin and airway inflammation, this newly found mechanism of Act1 also provides an opportunity to develop new IL-17–Act1-targeted therapeutic agents for treating inflammatory diseases.

Methods

Methods, including statements of data availability and any associated accession codes and references, are available at https://doi.org/10.1038/s41590-018-0071-9.

Received: 26 June 2017; Accepted: 16 February 2018;
Published online: 21 March 2018

© 2018 Nature America Inc., part of Springer Nature. All rights reserved.

References

1. Harrington, L. E. et al. Interleukin 17-producing CD4+ effector T cells develop via a lineage distinct from the T helper type 1 and 2 lineages. *Nat. Immunol.* **6**, 1123–1132 (2005).
2. Park, H. et al. A distinct lineage of CD4 T cells regulates tissue inflammation by producing interleukin 17. *Nat. Immunol.* **6**, 1133–1141 (2005).
3. Cua, D. J. & Tato, C. M. Innate IL-17-producing cells: the sentinels of the immune system. *Nat. Rev. Immunol.* **10**, 479–489 (2010).
4. Kolls, J. K. & Khader, S. A. The role of Th17 cytokines in primary mucosal immunity. *Cytokine Growth Factor Rev.* **21**, 443–448 (2010).
5. Patel, D. D., Lee, D. M., Kolbinger, F. & Antoni, C. Effect of IL-17A blockade with secukinumab in autoimmune diseases. *Ann. Rheum. Dis.* **72**, iii116–iii123 (2012).
6. Swaidani, S. et al. The critical role of epithelial-derived Act1 in IL-17- and IL-25-mediated pulmonary inflammation. *J. Immunol.* **182**, 1631–1640 (2009).
7. Toy, D. et al. Cutting edge: interleukin 17 signals through a heteromeric receptor complex. *J. Immunol.* **177**, 36–39 (2006).
8. Shen, F. & Gaffen, S. L. Structure-function relationships in the IL-17 receptor: implications for signal transduction and therapy. *Cytokine* **41**, 92–104 (2008).
9. Novatchkova, M., Leibbrandt, A., Werzowa, J., Neubüser, A. & Eisenhaber, F. The STIR-domain superfamily in signal transduction, development and immunity. *Trends Biochem. Sci.* **28**, 226–229 (2003).
10. Li, X. et al. Act1, an NF-κB-activating protein. *Proc. Natl Acad. Sci. USA* **97**, 10489–10493 (2000).
11. Chang, S. H., Park, H. & Dong, C. Act1 adaptor protein is an immediate and essential signaling component of interleukin-17 receptor. *J. Biol. Chem.* **281**, 35603–35607 (2006).
12. Qian, Y. et al. The adaptor Act1 is required for interleukin 17-dependent signaling associated with autoimmune and inflammatory disease. *Nat. Immunol.* **8**, 247–256 (2007).
13. Gu, C., Wu, L. & Li, X. IL-17 family: cytokines, receptors and signaling. *Cytokine* **64**, 477–485 (2013).
14. Stoecklin, G., Mayo, T. & Anderson, P. ARE-mRNA degradation requires the 5′-3′ decay pathway. *EMBO Rep.* **7**, 72–77 (2006).
15. Leppek, K. et al. Roquin promotes constitutive mRNA decay via a conserved class of stem-loop recognition motifs. *Cell* **153**, 869–881 (2013).
16. Stumpo, D. J., Lai, W. S. & Blackshear, P. J. Inflammation: cytokines and RNA-based regulation. *Wiley Interdiscip. Rev. RNA* **1**, 60–80 (2010).
17. Schoenberg, D. R. & Maquat, L. E. Regulation of cytoplasmic mRNA decay. *Nat. Rev. Genet.* **13**, 246–259 (2012).
18. Mino, T. et al. Regnase-1 and roquin regulate a common element in inflammatory mRNAs by spatiotemporally distinct mechanisms. *Cell* **161**, 1058–1073 (2015).
19. Brennan, C. M. & Steitz, J. A. HuR and mRNA stability. *Cell. Mol. Life Sci.* **58**, 266–277 (2001).
20. Herjan, T. et al. HuR is required for IL-17-induced Act1-mediated CXCL1 and CXCL5 mRNA stabilization. *J. Immunol.* **191**, 640–649 (2013).
21. Erickson, S. L. & Lykke-Andersen, J. Cytoplasmic mRNP granules at a glance. *J. Cell Sci.* **124**, 293–297 (2011).
22. Anderson, P., Kedersha, N. & Ivanov, P. Stress granules, P-bodies and cancer. *Biochim. Biophys. Acta* **1849**, 861–870 (2015).
23. Velichko, S. et al. A novel nuclear function for the interleukin-17 signaling adaptor protein Act1. *PLoS One* **11**, e0163323 (2016).
24. Liu, C. et al. A CC' loop decoy peptide blocks the interaction between Act1 and IL-17RA to attenuate IL-17- and IL-25-induced inflammation. *Sci. Signal.* **4**, ra72 (2011).
25. Hartupee, J., Liu, C., Novotny, M., Li, X. & Hamilton, T. IL-17 enhances chemokine gene expression through mRNA stabilization. *J. Immunol.* **179**, 4135–4141 (2007).
26. Datta, S. et al. IL-17 regulates CXCL1 mRNA stability via an AUUUA/tristetraprolin-independent sequence. *J. Immunol.* **184**, 1484–1491 (2010).
28. Wang, Z., Jiao, X., Carr-Schmid, A. & Kiledjian, M. The hDcp2 protein is a mammalian mRNA decapping enzyme. *Proc. Natl Acad. Sci. USA* **99**, 12663–12668 (2002).
29. She, M. et al. Structural basis of dcp2 recognition and activation by dcp1. *Mol. Cell* **29**, 337–349 (2008).
30. Rzeczkowski, K. et al. c-Jun N-terminal kinase phosphorylates DCP1a to control formation of P bodies. *J. Cell Biol.* **194**, 581–596 (2011).
31. Aizer, A., Kafri, P., Kalo, A. & Shav-Tal, Y. The P body protein Dcp1a is hyper-phosphorylated during mitosis. *PLoS One* **8**, e49783 (2013).
32. Bulek, K. et al. The inducible kinase IKKi is required for IL-17-dependent signaling associated with neutrophilia and pulmonary inflammation. *Nat. Immunol.* **12**, 844–852 (2011).
33. Qu, F. et al. TRAF6-dependent Act1 phosphorylation by the IκB kinase-related kinases suppresses interleukin-17-induced NF-κB activation. *Mol. Cell. Biol.* **32**, 3925–3937 (2012).
34. Zhong, X.-Y., Wang, P., Han, J., Rosenfeld, M. G. & Fu, X.-D. SR proteins in vertical integration of gene expression from transcription to RNA processing to translation. *Mol. Cell* **35**, 1–10 (2009).
35. Bresson, S., Tuck, A., Staneva, D. & Tollervey, D. Nuclear RNA decay pathways aid rapid remodeling of gene expression in yeast. *Mol. Cell* **65**, 787–800.e5 (2017).
36. Sun, D. et al. Treatment with IL-17 prolongs the half-life of chemokine CXCL1 mRNA via the adaptor TRAF5 and the splicing-regulatory factor SF2 (ASF). *Nat. Immunol.* **12**, 853–860 (2011).
37. Huynh, N. et al. Allosteric interactions direct binding and phosphorylation of ASF/SF2 by SRPK1. *Biochemistry* **48**, 11432–11440 (2009).
38. Tiedje, C. et al. The p38/MK2-driven exchange between tristetraprolin and HuR regulates AU-rich element-dependent translation. *PLoS Genet.* **8**, e1002977 (2012).
39. Chesné, J. et al. Prime role of IL-17A in neutrophilia and airway smooth muscle contraction in a house dust mite–induced allergic asthma model. *J. Allergy Clin. Immunol.* **135**, 1643–1645.e5 (2015).
40. Liu, C. et al. The flavonoid cyanidin blocks binding of the cytokine interleukin-17A to the IL-17RA subunit to alleviate inflammation in vivo. *Sci. Signal.* **10**, eaaf8823 (2017).
41. Ryzhakov, G. & Randow, F. SINTBAD, a novel component of innate antiviral immunity, shares a TBK1-binding domain with NAP1 and TANK. *EMBO J.* **26**, 3180–3190 (2007).
42. Chau, T.-L. et al. Are the IKKs and IKK-related kinases TBK1 and IKK-epsilon similarly activated? *Trends Biochem. Sci.* **33**, 171–180 (2008).
43. Nakatsu, Y. et al. Functionally distinct effects of the C-terminal regions of IKKε and TBK1 on type I IFN production. *PLoS One* **9**, e94999 (2014).
44. Helgason, E., Phung, Q. T. & Dueber, E. C. Recent insights into the complexity of Tank-binding kinase 1 signaling networks: the emerging role of cellular localization in the activation and substrate specificity of TBK1. *FEBS Lett.* **587**, 1230–1237 (2013).

Acknowledgements

We thank J. Lykke-Andersen (University of California, San Diego) as well as V. Heissmeyer (Biomedical Center Munich) and M. Kiledjian (Rutgers University) for plasmids. We thank T. Maniatis (Columbia University Medical Center) and E. Izaurralde (Max Planck Institute for Developmental Biology) for providing materials. This work was supported by the US National Institutes of Health (P01HL103453, P01 CA062220 to X.L. and P01 HL 029582 to P.L.F/X.L.) and a grant from NMSS (RG5130A2/1 to X.L.).

Author contributions

T.H. and L.H. designed experiments, performed experiments, analyzed data and wrote the manuscript with input from the coauthors. J.B., K.B., W.Q., C.L., Xiao Li, X.C., H.Y., S.O., H.Z., J.Z., V.K. and E.C. assisted with experiments and participated in discussion. M.A., K.A., D.D.L., J.Q., P.L.F. and T.A.H. facilitated the experimentation and offered critical scientific discussion. Xiaoxia Li and D.D. designed experiments, analyzed data and wrote the manuscript with input from the coauthors.

Competing interests

The authors declare no competing interests.

Additional information

Supplementary information is available for this paper at https://doi.org/10.1038/s41590-018-0071-9.

Reprints and permissions information is available at www.nature.com/reprints.

Correspondence and requests for materials should be addressed to X.L.

Publisher's note: Springer Nature remains neutral with regard to jurisdictional claims in published maps and institutional affiliations.

© 2018 Nature America Inc., part of Springer Nature. All rights reserved.

Methods

Animals. IKKi-deficient mice were a gift from T. Maniatis. TBK1 flox mice were obtained from Millenium Pharmaceuticals. Mice 6 weeks of age were used for primary kidney cell isolation. LSL–HA–Act1 knock-in mice were bred with UBC-Cre-ERT2 mice[45]. All mice were on the C57BL/6 N background; all protocols were approved by the Cleveland Clinic Institutional Animal Care and use Committee, and all studies were executed by following relevant ethical regulations detailed in animal-use protocols.

Cell culture and reagents. The following antibodies were used: Santa Cruz Biotechnology, anti-Act1 (sc-11444, clone H300), anti-HuR (sc-5261, clone 3A2), anti-SF2 (anti-28724, clone H-110), anti-GAPDH (sc-47724, mouse monoclonal) and anti-β-actin (sc-8432, mouse monoclonal); Sigma, anti-HA (H-9658, mouse monoclonal); Cell Signaling Technology, anti-TBK1 (3504, clone D1B4), anti-M2 (2368, rabbit polyclonal), anti-V5 (13202, rabbit polyclonal), anti-p-JNK (9251, rabbit polyclonal), anti-JNK (9252, rabbit polyclonal), anti-p-IκB (2859, clone 14D4), anti-p-p65 (3033, clone 93H1), anti-p65 (8242, clone D14E12), anti-Ikki (3416, clone D61F9), anti-p-IKKα/β (2697, clone 16A6) and anti-pERK (3371, rabbit polyclonal); Milipore, normal mouse IgG (12-371) and normal rabbit IgG (12-370) . Antibody to p-S315 Dcp1a was kind gift from E. Izaurralde. Antibody to Dcp1 was kind gift from J. Lykke Andersen. Goat anti-rabbit IgG-HRP (Cell Signaling Technology 7074, polyclonal) and goat anti-mouse IgG-HRP (Cell Signaling Technology, 7076, polyclonal) were used as secondary antibodies for immunoblot analysis. TBK1 inhibitor MRT67307 was purchased from Sigma Aldrich. Primary MEFs were isolated from wild-type, Act1-deficient and LSL–HA–Act1 knock-in/UBC-Cre-ERT2 embryos at embryonic day 14. Cell culture of MEFs, HeLa Tet-Off cells and primary kidney epithelial cells was performed as previously described[20,24]. Proximity-based ligation assays were performed in HeLa cells according to the manufacturer's instructions (Duolink Assay, Sigma Aldrich).

For stimulation ex vivo, cells were treated with mouse IL-17A (50 ng/ml, 421-MT, R&D Systems), human IL-17A (50 ng/ml, 317-1 ML, R&D Systems), or mouse TNF (10 ng/ml, 410-MT, R&D Systems), IL-1 (10 ng/ml, 201-LB, R&D Systems) or IL-25E (10 μg/ml, 1399-IL, R&D Systems).

Transfection, adenoviral and retroviral infection. Transfections of HeLa cells were conducted with Lipofectamine 2000 (Invitrogen) according to the manufacturer's instructions. For Act1 reconstitution into *Act1*$^{-/-}$ MEFs and transfection of LSL–HA–Act1 knock-in/UBC-Cre-ERT2 MEFs, cells were either infected by retroviral supernatant as described previously[12] or transfected with an Amaxa nucleofector apparatus. Supernatants for retroviral infections were obtained by transfecting Phoenix cells with 5 μg of retroviral constructs derived from pMSCV-IRES-GFP for 48 h. MEFs were infected with viral supernatant for 24 h, and GFP-positive cells were sorted out to establish stable cell lines for downstream assays. Transfections with the Amaxa nucleofector apparatus were performed according to the manufacturer's instructions (program A-023, Amaxa MEF Nucleofector Kit 1).

Quantitative real-time PCR. Total RNA was isolated with TRIzol reagent (Invitrogen). The cDNA was synthesized with random hexamers (Applied Biosystems) and M-MLV reverse transcriptase (Promega). Real-time PCR was performed with a SYBR Green PCR Master Mix kit (Applied Biosystems). All gene expression results were calculated by the change in cycling threshold (ΔCt) method, where ΔCt = Ct of target gene − Ct of *Actb* (encoding β-actin), and are presented as $2^{-\Delta Ct}$. The primers used for qPCR are listed in Supplementary Table 1.

Constructs. For GFP reporter constructs, full-length cDNAs of hAct1, hDcp1a, hIKKi, hTBK1 and hTIA1 were cloned into the pEGFP-N1 vector (Clontech). For RFP reporter constructs, full-length cDNAs of hAct1, hIRAK1 and hDcp1a were cloned into pDsRed-Monomer-Hyg-N1 vector (Clontech). For constructs V5-hDcp1a, FLAG-hDcp1a, FLAG-hDcp2, FLAG-hIRAK1, V5-IL-17RA, HA-hAct1 and HA-hAct1ΔSEFIR, the cDNAs with the corresponding tag were cloned into the pcDNA3.1 vector. Wild-type (FLAG-hAct1) and Act1 internal-deletion mutants of the SEFIR domain (designated ΔSEFIR1 to ΔSEFIR5 (based on the five exons that encode regions of the SEFIR domain: 410 to 439, 440 to 462, 463 to 501, 502 to 526, and 527 to 552) and ΔSEFIR (deletion of amino acid residues 391–537)), receptor binding mutant[41] (H472D), TRAF6 binding mutant[41] (deletion of amino acid residues 38–42, 333–337) or RNA binding mutant (SEFIR1 + 5mt) (K407A, K524A, K526A and K527A) were FLAG-tagged and cloned into pcDNA3.1. Retroviral Act1-WT and Act1-mutant constructs derived from pMSCV-IRES-GFP were as previously described[6,12,24].

Constructs for in vitro transcription. Fragments containing the 3′-UTR sequences of CXCL1 220 (nt 720–940) and the truncated fragments CXCL1 120 (nt 780–900), CXCL1 110 (nt 780–890), CXCL1 90 (nt 790–880), CXCL1 80 (nt 800–880), CXCL1 70 (nt 800–870); SBE WT (CXCL1 47, nt 810–857), SBE mutant B (CXCL1 47, nt 810–857 with altered sequence shown in Supplementary Table 2), SBE mutant C (CXCL1 47, nt 810–857 with altered sequence shown in Supplementary Table 2), stem-loop B (CXCL1, 800-835) and stem-loop C (CXCL1, 830–856), as well as the 3′-UTR sequences of TNF (nt 1361–1507), GM-CSF (nt 513–785) and GPx4 (nt 775–962), were generated by PCR and cloned into the pGEM-3ZF(+) vector (Promega) through the EcoRI and BamHI sites. The plasmid containing the 3′ UTR of mouse TNF was a kind gift from V. Heissmeyer. All mutations were introduced with a QuikChange II Site Directed Mutagenesis Kit (Stratagene) according to the manufacturer's instructions. Primers used for generating all constructs are listed in Supplementary Table 2.

In vitro transcription and cap labeling. REMSA radiolabeled 3′-UTR RNA probes were synthesized from BamHI-linearized plasmid templates (described in 'Constructs for in vitro transcription') with T7 RNA polymerase and 1 mM GTP, 1 mM ATP, 1 mM CTP, 0.005 mM UTP and 25 μCi of ^{32}P-labeled UTP for 3 h at 37 °C. Probes were DNase I treated for 20 min and then phenol–chloroform extracted. The aqueous phase was passed through a Micro Bio-Spin P30 column according to the manufacturer's instructions (Bio-Rad). For in vitro decapping, probes were synthetized as above, but with unlabeled 1 mM CTP, then DNase treated and purified. Cap labeling was performed with the Vaccinia Capping System (NEB) according to the manufacturer's instructions in the presence of [α-^{32}P]GTP.

For RNase footprinting experiments, cold synthetic transcripts were dephosphorylated with SuperSAP (Affymetrix), purified and resuspended in nuclease-free water. Dephosphorylated transcripts were end-labeled in the presence of [γ-^{32}P]ATP (3,000 Ci/mmol; Perkin Elmer Easy Tides) and T4 PNK (NEB) at 20 units/pmol RNA. The transcripts were gel purified on 8% acrylamide (19:1)/7 M urea gels and eluted in 10 mM Tris-HCl, pH 7.5, 1 mM EDTA, pH 8, and 300 mM NaOAc, pH 5.5, at 4 °C overnight. Purified RNA was stored in 10 mM Tris-HCl, pH 7.5, at −20 °C.

RNase footprinting. ^{32}P-end-labeled CXCL1 SBE RNA was heated to 95 °C and slow cooled to room temperature. The RNA (2.5 nM) was incubated in L30 binding buffer (30 mM Tris-HCl, pH 8.0, 75 mM KCl, 5 mM $MgCl_2$, 1 mM DTT, 0.04 μg/μl BSA (NEB), 10% glycerol and 50 ng/μl yeast tRNA) with or without mouse Act1 SEFIR protein (1.5 μM) at 30 °C for 10 min. Reactions were cooled to room temperature over a 2-min period and then placed at 22 °C for 2–5 min. The indicated amounts of RNase T1, A or V1 (Ambion) were added to the appropriate samples and incubated at 22 °C for 5 min. Enzymatic reactions were quenched with 30 μl Inactivation/Precipitation buffer (Ambion) and purified according to the manufacturer's directions. Samples were resuspended in 10 μl of loading buffer (Ambion), heat denatured at 95 °C for 5 min and separated in a denaturing 8% (19:1) polyacrylamide/7 M urea gel. The dried gels were visualized with a phosphorimager or on film.

Sequencing ladders were prepared by incubating ^{32}P-end-labeled *Cxcl1* SBE RNA (2.5 nM) in 1× Sequencing Buffer (Ambion) supplemented with 50 ng/μl yeast tRNA. The RNAs were incubated at 50 °C for 5 min and cooled to 22 °C, and the indicated amounts of RNases T1 and A were then added. The samples were incubated, quenched and purified as described above. Alkali ladders were prepared by incubating ^{32}P-end-labeled *PHGPx* SECIS RNA (2.5 nM) in 100 mM NaOH, 2 mM EDTA, pH 8.0, and 2 μg/μl yeast tRNA at 37 °C for 3 min, to which 0.2 M Tris-HCl, pH 8.0 (final) was added. The samples were frozen on dry ice and combined with an equal volume of loading buffer.

RNA electrophoretic mobility shift assay (REMSA). Increasing amounts of purified protein and labeled probes (10 fmol; described in 'In vitro transcription') were combined in the binding buffer for 30 min. The final REMSA binding-buffer concentrations were 140 mM KCl, 10 mM HEPES, pH 7.9, 5% glycerol, 1 mM DTT and 0.33 mg/ml tRNA. The reaction was further supplemented with 15 μg salmon sperm DNA to decrease nonspecific interactions from the lysate. Complexes were resolved on either 4% or 6% nondenaturing polyacrylamide gels. The gels were dried, and the appearance of complexes was visualized by exposure to BioMax MR film. Dissociation constants were determined by quantifying the protein-bound fractions in ImageJ software and were plotted against protein concentration (nM). K_d values were extracted from plots fitted to a hyperbolic function in GraphPad Prism software (OriginLab).

SBE aptamer competition. The purified recombinant His-MBP-Act1 SEFIR (200 ng) was incubated with the ^{32}P-labeled *Csf2* and *Tnf* 3′-UTR probes for 15 min to form protein–RNA complexes. Cold RNAs were added at 0-, 25-, 50-, 100- or 200-fold molar excess over the probe for an additional 10 min, then subjected to REMSA. SBE WT (*Cxcl1* 47, as indicated in Fig. 3a) and SBE mutant C were used in the competition assay (Fig. 7a and d). IC_{50} values were calculated as the concentration of aptamers that displaced 50% of bound *Cxcl1* 220 probe from the Act1 SEFIR.

Protein modeling. The structure model of Act1 SEFIR was built in SWISS-Model (http://swissmodel.expasy.org/), by using the crystal structure of IL-17RA SEFIR as the template[46] (PDB 4NUX).

Surface plasmon resonance. The SPR binding affinity was analyzed on a BIAcore 3000 instrument. The biotinylated RNA was immobilized on a streptavidin-coated

© 2018 Nature America Inc., part of Springer Nature. All rights reserved.

sensor chip, which was activated and blocked according to standard protocols. RNA was diluted to 1 mM in HBS-EP buffer (10 mM HEPES, pH 7.4, 150 mM NaCl, 3 mM EDTA and 0.005% surfactant P20) heated at 80 °C for 10 min, cooled to room temperature to allow for annealing of the stem and diluted 500-fold in running buffer. RNA was injected at a flow rate of 10 µl/min, and ~40 resonance units of RNA were captured on the chip. To study the RNA–Act1 interactions, the proteins were diluted in running buffer and injected at the concentrations indicated in the sensorgrams. Binding experiments were carried out at 25 °C and a flow rate of 30 µl/min. Any protein that remained bound after a 3-min dissociation phase was removed by injection of 2 M NaCl for 60 s at 20 µl/min, thus regenerating the RNA surface completely. Data were analyzed with BIAcore 3000 evaluation software, and curves were fitted with the '1:1 binding with drifting baseline' model.

Immunodepletion of endogenous TBK1 and IKKi. TBK1- or IKKi-depleted extracts were prepared by incubating extracts of 2×10^6 of HeLa cells with 25 µl protein G beads (preincubated with 5 µg of either anti-TBK1 or anti-IKKi antibodies) at 4 °C for 4 h. The beads were then separated from the extract by centrifugation at 3,000 g for 2 min at 4 °C, and supernatants were used for protein purification.

Decapping assays. Dcp1–Dcp2 complex and Act1 protein were purified from HeLa cells (2×10^6) either cotransfected with 10 µg of FLAG-tagged Dcp1 and FLAG-tagged Dcp2 (kind gift from J. Lykke Andersen) or with 10 µg of FLAG-tagged Act1, by using anti-FLAG/M2-beads (Sigma) and eluted in 50 µl with 3× FLAG peptide (Sigma), and protein concentrations were estimated by comparison to an Act1 SEFIR protein of known concentration. 10 fmol of ^{32}P-cap-labeled RNA substrate was incubated with the purified Dcp1–Dcp2 complex (100 ng of each protein) and increasing amounts of purified Act1 protein (0, 100 and 300 ng) in decapping buffer (10 mM Tris, pH 7.5, 100 mM KOAc, 2 mM MgOAc and 2 mM DTT) supplemented with fresh 0.5 mM $MnCl_2$ for 30 min at 370 °C. The reaction was terminated by addition of 1 µl of 0.5 M EDTA. Reaction products were separated and identified by TLC on cellulose sheets developed in 450 mM $(NH4)_2SO_4$. m^7GMP and m^7GDP (20 µg) were spotted routinely on TLC plates along with reaction samples to serve as markers that could be visualized by UV shadowing.

Intradermal injection. LSL–HA–Act1 knock-in/UBC-Cre-ERT2 mice were injected with tamoxifen (~5 mg/25 g weight) 14 and 7 d before intradermal experiments. The ears of 8-week-old female mice were injected intradermally with 20 µl of PBS alone or with PBS containing 0.5 mg of recombinant mouse IL-17A in the presence or absence of 5 nmol of either SBE WT aptamer or SBE mutant C aptamer (sequence in Supplementary Table 2). Mice were injected daily for 6 consecutive days. Six days after injection, skin tissue was collected for RNA and staining analyses. For H&E and 3,3′-diaminobenzidine (DAB; BD Phamagen) staining, skin tissue was fixed in 10% formalin and then processed into paraffin blocks. Epidermal thickness was quantified in ImageJ software.

HDM-induced asthma. Eight-week-old female WT C57BL/6 mice were sensitized subcutaneously with HDM (100 mg/mouse; *Dermatophagoides farina*, Greer Laboratories) in complete Freund's adjuvant (CFA) on day 0 and subsequently challenged (intranasally) with HDM (100 mg per mouse) on day 14. One hour before the last HDM challenge, mice were administered intranasally with either SBE WT or SBE mutant C aptamer mixed with 5 µl of TransIT-TKO reagent (Mirus Bio) and PBS in a total volume of 40 µl. We equally divided the aptamer mix and into two nostrils and applied it with a micropipette. Each mouse received 5 nmol of aptamer. BAL cell counting and tissue collection were performed 24 h after the last HDM challenge.

For monitoring aptamer delivery into the trachea, fluorescently labeled SBE WT aptamers were intranasally delivered to tamoxifen-treated LSL-Act1-HA knock-in Cre-ERT2 mice (described in 'Intradermal injection').

Aptamer design. Aptamers containing sequences of SBE WT and SBE mutant C (Supplementary Table 3) were ordered from Integrated DNA Technologies. Three first residues form both the 5′ and the 3′end were methylated (2′-*O*-methyl RNA bases) to enhance stability. For detection, aptamers were further modified at their 5′ ends with either 6-FAM or Atto647 fluorescent dyes.

Histological analysis. Tracheas were collected from LSL-Act1-HA KI Cre-ERT2 mice subjected to intranasal administration of fluorescently labeled SBE RNA aptamers, snap frozen in OCT medium and cryosectioned at 5 µm. Frozen tissue sections were fixed and permeabilized with 4% paraformaldehyde solution containing 0.2% Triton X-100 for 10 min. Sections were incubated with rabbit anti-HA antibody, then subjected to staining with Alexa Fluor 488-conjugated goat anti-mouse antibody (green) and microscopic analysis.

ELISA. Supernatants from cell cultures were collected, and the levels of mouse cytokines CXCL1 and TNF were measured with Duoset ELISA kits (R&D System) according to the manufacturer's instructions.

RNA binding assays and RIP. The ability of Act1 to bind to RNA in vivo was assessed as described previously[47]. Briefly, 10×10^6 *Act1*$^{-/-}$ MEFs reconstituted by retroviral infection with M2-tagged mouse wild-type Act1 were left untreated or treated with IL-17 (50 ng/ml) for 1 h. Cells were trypsinized, washed twice and resuspended in 10 ml ice-cold PBS. Cells were fixed in 0.1% formaldehyde for 15 min at room temperature, whereupon the cross-linking reaction was stopped with glycine (pH 7; 0.25 M). The cells were then washed twice with ice-cold PBS, resuspended in 2 ml RIPA buffer (50 mM Tris-HCl, pH 7.5, 1% Nonidet P-40, 0.5% sodium deoxycholate, 0.05% SDS, 1 mM EDTA, 150 mM NaCl and proteinase inhibitors) and sonicated. The lysate was centrifuged (15 min, 4 °C, 16,000 *g*), and 1 ml of each supernatant was immunoprecipitated overnight at 4 °C with Dynabeads (Invitrogen) preincubated with 20 µg anti-M2 or anti-IgG antibody. The beads were washed five times with 1 ml RIPA buffer and resuspended in 150 µl elution buffer (50 mM Tris-Cl, pH 7, 5 mM EDTA, 10 mM DTT and 1% SDS). Cross-linking was reversed by incubation at 70 °C for 45 min. RNA was purified from immunoprecipitates with TRIzol (Invitrogen) according to the manufacturer's instructions and treated with RNase-free DNase. The cDNAs were synthesized, and 10% (2 µl) of the reverse transcriptase product was subjected to quantitative real-time PCR. Primers used for quantitative real-time PCR are listed in Supplementary Table 1.

RIP data analysis. The Ct value of each RIP RNA fraction was normalized to the input-RNA-fraction Ct value for the same qPCR Assay (ΔCt) to account for RNA sample-preparation differences. Then the normalized RIP-fraction Ct value (ΔCt) was adjusted for the normalized background (anti-IgG) (nonspecific (NS) antibody)-fraction Ct value (ΔΔCt). The fold enrichment (RIP/NS) was calculated by linear conversion of the ΔΔCt. Below are the formulas used for the calculation: $\Delta Ct_{\text{normalized RIP}} = Ct_{\text{RIP}} - (Ct_{\text{input}} - \log_2(\text{fraction of the input RNA saved}))$; $\Delta\Delta Ct_{\text{RIP/NS}} = \Delta Ct_{\text{normalized RIP}} - \Delta Ct_{\text{normalized NS}}$; fold enrichment $= 2^{-\Delta\Delta Ct RIP/NS}$.

Immunoblotting, immunoprecipitation and nuclear fractionation. Cells were harvested and lysed on ice in a lysis buffer containing 0.5% Triton X-100, 20 mM HEPES, pH 7.4,150 mM NaCl, 12.5 mM β-glycerophosphate, 1.5 mM $MgCl_2$, 10 mM NaF, 2 mM dithiothreitol, 1 mM sodium orthovanadate, 2 mM EGTA, 20 mM aprotinin and 1 mM phenylmethylsulfonyl fluoride for 20 min, then subjected to centrifugation at 12,000 r.p.m. for 15 min to extract clear lysates. For immunoprecipitation, cell lysates were incubated with 1 µg of antibody and Protein A–Sepharose beads at 4 °C overnight. After incubation, the beads were washed four times with lysis buffer, and the precipitates were eluted with 2× sample buffer. Eluates and whole cell extracts were resolved on SDS–PAGE, then subjected to immunoblotting. Nuclear fractionation was performed with a NUCLEI EZ PREP kit purchased from Sigma in accordance with the manufacturer's instructions. Nuclear pellets were suspended in 30 µl of nuclear extraction buffer (20 mM HEPES, 400 mM NaCl, 1 mM EDTA and 1 mM EGTA in water, pH 7.9) containing freshly prepared 1 mM DTT and protease-inhibitor cocktail. After a 1.5-h incubation on an ice bath with intermittent vortexing, extracts were centrifuged, and supernatant was collected for immunoprecipitation. Uncropped gels pertaining to all figures can be found in Supplementary Fig. 8.

Expression and purification of His-IL-17RA SEFIR, His-MBP-mAct1 SEFIR and His-MBP proteins. The cDNA encoding a SEFIR domain–containing fragment of human IL17RA (His-IL-17RA SEFIR, residues 351–616) was cloned into a modified pET-28 vector, with an N-terminal hexahistidine tag and a tobacco etch virus protease (TEV)-recognition site (ENLYFQG). The IL17RA SEFIR domain was expressed and purified by double nickel–nitrilotriacetic acid affinity methods as previously described[48]. Size-exclusion chromatography on a Superdex s200 high-resolution column was used as a final step for purification. The cDNA encoding a SEFIR domain containing a fragment of mouse Act1 (residues 391–537) and its deletion mutants of the SEFIR domain, designated SEFIR1–SEFIR5 (according to the five exons that encode regions of the SEFIR domain: 410–439, 440–462, 463–501, 502–526 and 527–552) was cloned into a modified pET28b vector for expression of MBP with an N-terminal hexahistidine tag and a C-terminal TEV-recognition site. Recombinant mAct1 SEFIR or MBP protein was expressed and purified as previously described[49]. Size-exclusion chromatography on a Superdex s200 high resolution column was used as a final step for purification.

In vitro kinase assay. Recombinant IKKi and TBK1 (100 nM) were incubated with purified SF2 and Dcp1(10 nM), respectively, in kinase assay buffer containing 25 mM Tris, pH 7.5, 5 mM β-glycerophosphate, 2 mM DTT, 0.1 mM Na_3VO_4 and 10 mM $MgCl_2$, supplemented with 100 nM ATP and 1 µl [γ-^{32}P]ATP (PerkinElmer) (10 µCi) at 37 °C for 30 min. The samples were subjected to SDS–PAGE, then autoradiography.

mRNA decay assay. Half-lives of endogenous mRNAs were determined with the use of actinomycin D (5 mg/ml) to inhibit transcription. Pulse–chase mRNA-decay assays in HeLa Tet-Off cells were performed as described previously[26]. The reporter RNA construct for this assay was obtained by cloning *Cxcl1* 220 (720–940) into pTRE2 (Clontech) containing the 5′ UTR and coding region of *Cxcl1*, as described previously[26] (KCΔ4). Transcription in the Tet-Off system is under control of

© 2018 Nature America Inc., part of Springer Nature. All rights reserved.

a tetracycline-response element. In the absence of tetracycline or its analog doxycycline, the tetracycline transactivator drives transcription of the reporter mRNA. After the addition of doxycycline to the culture medium, transcription is abolished, thus allowing for the rate of reporter mRNA decay to be measured. We treated the transfected cells with doxycycline to allow reporter *Cxcl1*mRNA to decay for 0, 45 and 90 min, and assessed remaining reporter mRNA encoding *Cxcl1* 220 and *Gapdh* mRNA. Total RNA was isolated with TRIzol reagent (Invitrogen) according to the manufacturer's instructions, then subjected to RT–PCR. The values were normalized to those of *Gapdh* mRNA.

Microscopy. Immunohistochemistry staining was recorded with an OLYMPUS DP71 digital camera attached to an Olympus BX41 microscope. Fluorescence images were captured with a Leica confocal Microscope (Lerner Institute Imaging Core). As a routine practice, three independent plates of cells were analyzed for quantification, with a total of 50 cells analyzed from each plate.

Statistical analyses. Statistical analysis was applied to biologically independent samples (separate plates of cells or mice) from every single experiment, and data were not pooled from independent experiments for statistical analyses. Experiments were repeated at least twice, and the exact numbers of repeats are indicated in the figure legends. For all RT–PCR and ELISA analyses, at least three biological replicates (separate plates of cells) were used. Unless otherwise indicated, comparisons between two groups were analyzed by two-tailed Student's *t* tests. All bar graphs show mean and s.d. or s.e.m., as indicated in each legend. *P* values for comparisons are provided as exact values or as $P < 0.001$. Statistical analysis of mass spectrometry and microarray data are detailed in their respective sections. GraphPad Prism 7 was used for data analysis and representation.

Reporting Summary. Further information on experimental design is available in the Nature Research Reporting Summary linked to this article.

Data availability. The primary data for analysis of all figures and supplementary figures are available upon request.

References

27. Hartupee, J. et al. IL-17 signaling for mRNA stabilization does not require TNF receptor-associated factor 6. *J. Immunol.* **182**, 1660–1666 (2009).
45. Ruzankina, Y. et al. Deletion of the developmentally essential gene ATR in adult mice leads to age-related phenotypes and stem cell loss. *Cell Stem Cell* **1**, 113–126 (2007).
46. Zhang, B. et al. Structure of the unique SEFIR domain from human interleukin 17 receptor A reveals a composite ligand-binding site containing a conserved α-helix for Act1 binding and IL-17 signaling. *Acta Crystallogr. D Biol. Crystallogr.* **70**, 1476–1483 (2014).
47. Datta, S. et al. Tristetraprolin regulates CXCL1 (KC) mRNA stability. *J. Immunol.* **180**, 2545–2552 (2008).
48. Deng, J. et al. An improved protocol for rapid freezing of protein samples for long-term storage. *Acta Crystallogr. D Biol. Crystallogr.* **60**, 203–204 (2004).
49. Deng, J. et al. Structure of the ROC domain from the Parkinson's disease-associated leucine-rich repeat kinase 2 reveals a dimeric GTPase. *Proc. Natl Acad. Sci. USA* **105**, 1499–1504 (2008).

© 2018 Nature America Inc., part of Springer Nature. All rights reserved.

nature research

Corresponding author(s): Xiaoxia Li

Life Sciences Reporting Summary

Nature Research wishes to improve the reproducibility of the work that we publish. This form is intended for publication with all accepted life science papers and provides structure for consistency and transparency in reporting. Every life science submission will use this form; some list items might not apply to an individual manuscript, but all fields must be completed for clarity.

For further information on the points included in this form, see Reporting Life Sciences Research. For further information on Nature Research policies, including our data availability policy, see Authors & Referees and the Editorial Policy Checklist.

Please do not complete any field with "not applicable" or n/a. Refer to the help text for what text to use if an item is not relevant to your study.
For final submission: please carefully check your responses for accuracy; you will not be able to make changes later.

Experimental design

1. Sample size

   Describe how sample size was determined.

   Power analysis was performed to predetermine sample size of all in vivo experiments. Based on our previous studies (references below), we estimated the sample size (n=6) required to obtain 85% power for detecting a difference of 1.5 fold difference of mean between two groups at 0.05 level significance using Student t test. (minimum level of difference considered to be biologically relevant).
   References:
   2015 A Novel IL-17 Signaling Pathway Controlling Keratinocyte Proliferation and Tumorigenesis via the TRAF4–ERK5 Axis. Journal of Experimental Medicine 212(10):1571–1587
   2017 The Flavonoid Cyanidin Blocks Binding of the Cytokine Interleukin-17A to the IL-17RA Subunit to Alleviate Inflammation in Vivo. Sci. Signal. 10(467)

   In vitro: Power analysis was not performed to predetermine sample size. Instead, we determined the sample size based on related preliminary and published experiments (examples references below).
   References:
   Bulek, K. et al. The inducible kinase IKKi is required for IL-17-dependent signaling associated with neutrophilia and pulmonary inflammation. Nature immunology 12, 844 (2011).
   Herjan, T. et al. HuR is required for IL-17–induced Act1-mediated CXCL1 and CXCL5 mRNA stabilization. The Journal of Immunology 191, 640-649 (2013).
   Liu, C. et al. The flavonoid cyanidin blocks binding of the cytokine interleukin-17A to the IL-17RA subunit to alleviate inflammation in vivo. Sci. Signal. 10, eaaf8823 (2017).

2. Data exclusions

   Describe any data exclusions.

   no data was excluded

3. Replication

   Describe the measures taken to verify the reproducibility of the experimental findings.

   For intracellular imaging quantification 50 randomly cells chosen from 3 independent plates of were quantified.
   Every experiment shown was repeated at least three or two times as indicated in the figure legends. All of replicate experiments produced consistent, statistically significant data, as indicated in figure legends.
   For experiments involving purified proteins at least three batches of independently purified proteins were tested. For experiments involving cell lines at least three different batches of cells were tested.

4. Randomization

   Describe how samples/organisms/participants were allocated into experimental groups.

   Before treatment mice were randomly divided into experimental groups (8-weekold female C57BL/6J mice (n=6 mice/group)

5. Blinding

   Describe whether the investigators were blinded to group allocation during data collection and/or analysis.

   To reduce potential experimental bias, the identity of cell lines (MEFs expressing Act1 WT and its variants) identity of RNA aptamers, purified proteins as well as RNA probes (for REMSA) was blinded from the researchers performing the validation experiments. These identities were only revealed at the final data analysis stage.
   In case of the in vivo study RNA aptamer identity was blinded from researcher performing intranasal and intradermal injections. For the stage of tissue and BAL

fluid collection group allocation was concealed. These identities were only revealed at the final data analysis stage.

Note: all in vivo studies must report how sample size was determined and whether blinding and randomization were used.

6. Statistical parameters

For all figures and tables that use statistical methods, confirm that the following items are present in relevant figure legends (or in the Methods section if additional space is needed).

n/a	Confirmed
☐	☒ The exact sample size (*n*) for each experimental group/condition, given as a discrete number and unit of measurement (animals, litters, cultures, etc.)
☐	☒ A description of how samples were collected, noting whether measurements were taken from distinct samples or whether the same sample was measured repeatedly
☐	☒ A statement indicating how many times each experiment was replicated
☐	☒ The statistical test(s) used and whether they are one- or two-sided *Only common tests should be described solely by name; describe more complex techniques in the Methods section.*
☒	☐ A description of any assumptions or corrections, such as an adjustment for multiple comparisons
☐	☒ Test values indicating whether an effect is present *Provide confidence intervals or give results of significance tests (e.g. P values) as exact values whenever appropriate and with effect sizes noted.*
☐	☒ A clear description of statistics including central tendency (e.g. median, mean) and variation (e.g. standard deviation, interquartile range)
☐	☒ Clearly defined error bars in all relevant figure captions (with explicit mention of central tendency and variation)

See the web collection on statistics for biologists for further resources and guidance.

Software

Policy information about availability of computer code

7. Software

Describe the software used to analyze the data in this study.

Graphpad Prism 6.0, Microsfot Excel, ImageJ, BIAcore 3000.

For manuscripts utilizing custom algorithms or software that are central to the paper but not yet described in the published literature, software must be made available to editors and reviewers upon request. We strongly encourage code deposition in a community repository (e.g. GitHub). *Nature Methods* guidance for providing algorithms and software for publication provides further information on this topic.

Materials and reagents

Policy information about availability of materials

8. Materials availability

Indicate whether there are restrictions on availability of unique materials or if these materials are only available for distribution by a third party.

IKKi-deficient mice were a gift from T. Maniatis. TBK1 flox mice were obtained from Millenium Pharmaceuticals.
Dcp1-FLAG construct was obtained from Jens Lykke-Andersen (University of California, San Diego); construct containing 3'UTR of TNF mRNA was obtained from Vigo Heissmeyer (Biomedical Center Munich) and construct encoding hDcp2-FLAG was from Megerditch Kiledjian (Rutgers University). Remaining materials are commercially available as indicated in Materials and methods.

9. Antibodies

Describe the antibodies used and how they were validated for use in the system under study (i.e. assay and species).

p-S315 Dcp1a antibody was kind gift from Dr. Elisa Izaurralde. Dcp1 antibody was kind gift from Dr. Jens-Lykke Andersen. Specificity of above mentioned antibodies were validated and described in peer-reviewed publications, including:
2005 Multiple Processing Body Factors and the ARE Binding Protein TTP Activate mRNA Decapping. Molecular Cell 20(6): 905–915.
and
2011 C-Jun N-Terminal Kinase Phosphorylates DCP1a to Control Formation of P Bodies. The Journal of Cell Biology 194(4): 581–596.
The remaining antibodies used in this study can be found in the Materials & Methods section of this paper. Antibodies were validated according to the manufacturers instructions.

10. Eukaryotic cell lines

a. State the source of each eukaryotic cell line used.

HeLa cells were purchased from Clontech Laboratories

b. Describe the method of cell line authentication used.

All cell lines are periodically authenticated by STR analysis.

c. Report whether the cell lines were tested for mycoplasma contamination.

Cell lines were tested for mycoplasma contamination and were not contaminated.

d. If any of the cell lines used are listed in the database of commonly misidentified cell lines maintained by ICLAC, provide a scientific rationale for their use.

No commonly misidentified cell lines were used.

Animals and human research participants

Policy information about studies involving animals; when reporting animal research, follow the ARRIVE guidelines

11. Description of research animals

Provide all relevant details on animals and/or animal-derived materials used in the study.

All mice used for this study were on a C57BL/6 background. For special strains, the experimental mice were bred in house in SPF condition. Genotypes of these strains were confirmed using PCR analysis. For derivation of MEFs, embryos (E13.5 to E14.5) were used. Litter mates of the same gender carrying with control genotypes were used to derive control MEFs. Female mice between 6 to 8 weeks old purchased from Jackson lab were used for in vivo experiment (Figure 8).

Policy information about studies involving human research participants

12. Description of human research participants

Describe the covariate-relevant population characteristics of the human research participants.

This study did not involve human research participants.

nature immunology

SUPPLEMENTARY INFORMATION

https://doi.org/10.1038/s41590-018-0071-9

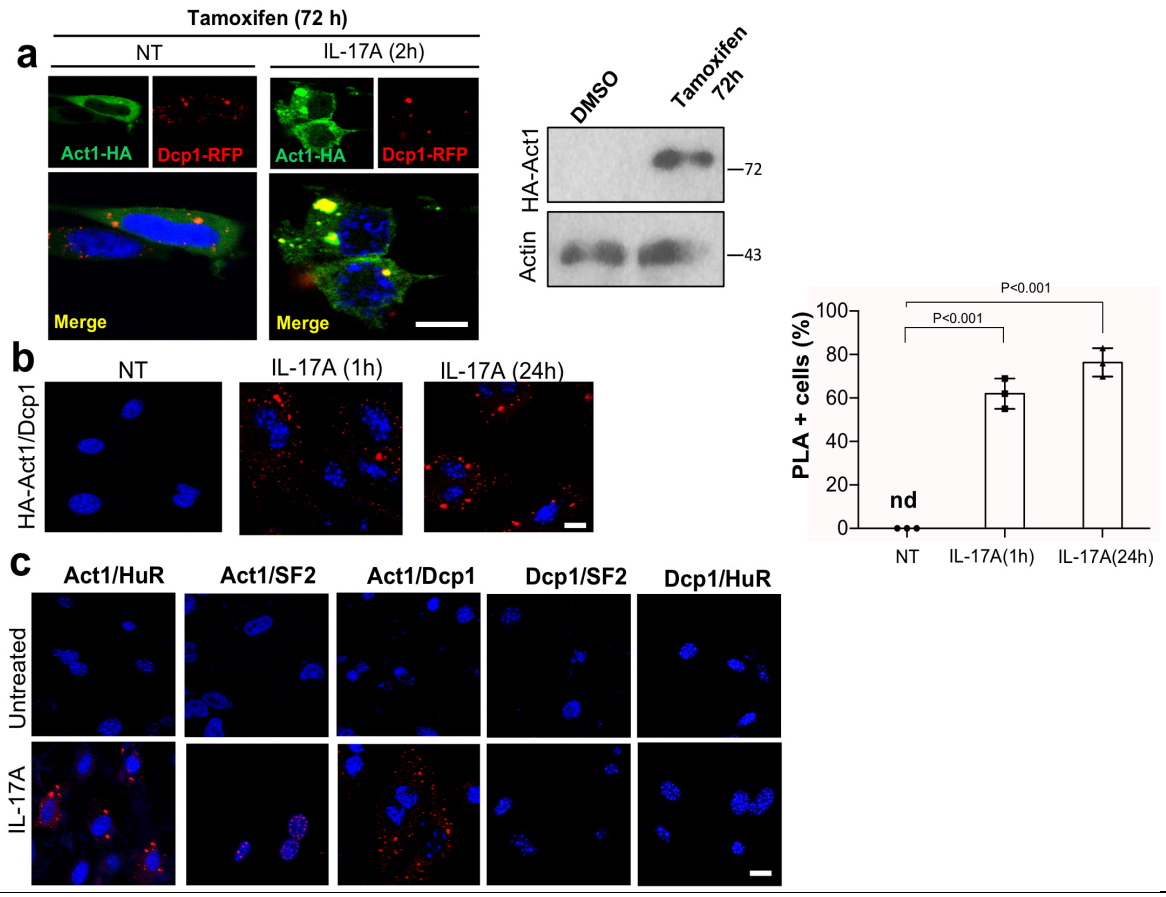
In the format provided by the authors and unedited.

IL-17-receptor-associated adaptor Act1 directly stabilizes mRNAs to mediate IL-17 inflammatory signaling

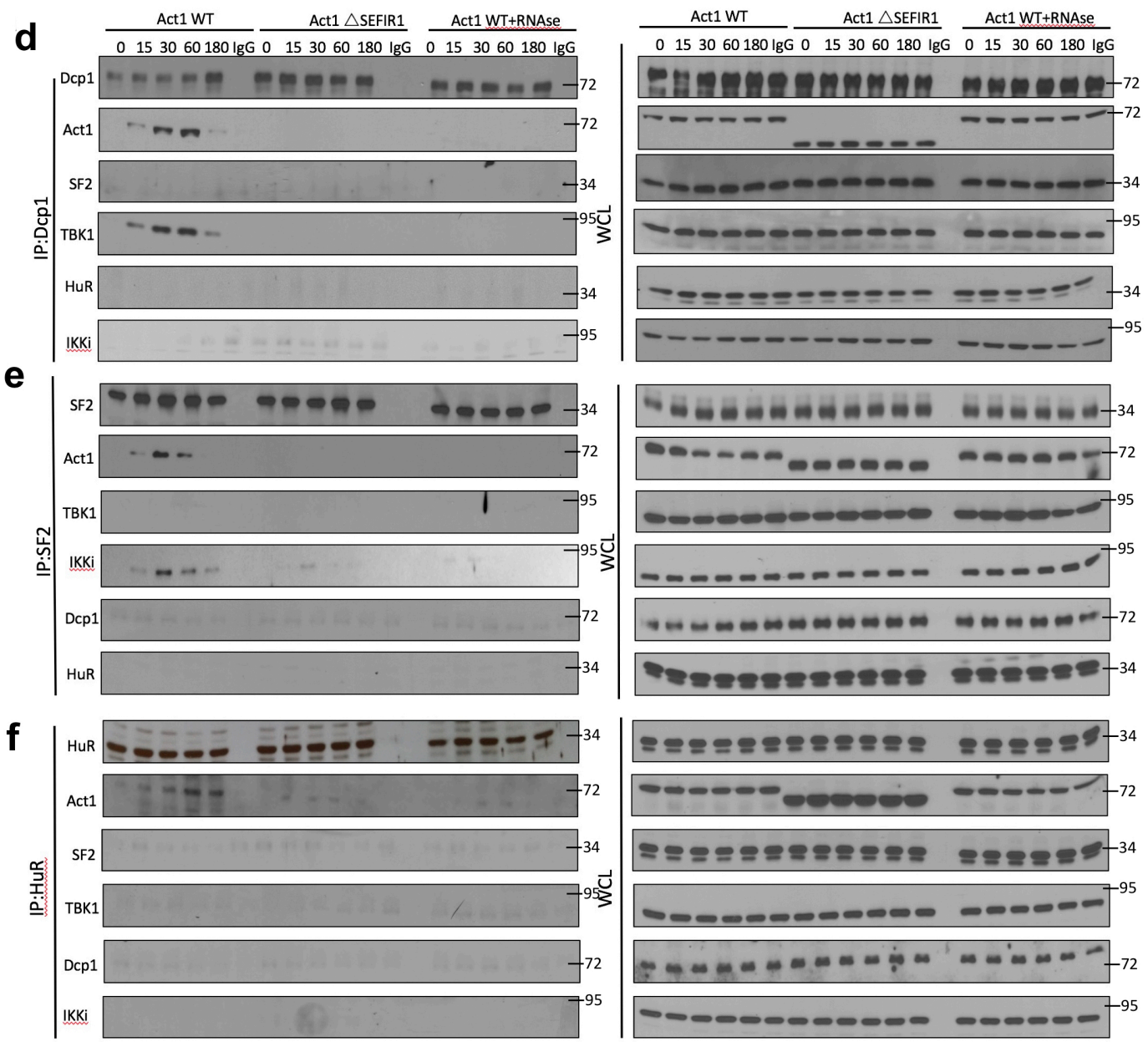
Tomasz Herjan[1,2,9], Lingzi Hong[1,9], Jodi Bubenik[3], Katarzyna Bulek[1,4], Wen Qian[1], Caini Liu[1], Xiao Li[5], Xing Chen[1], Hui Yang[1], Suidong Ouyang[1], Hao Zhou[1], Junjie Zhao[1], Kommireddy Vasu[3], Eric Cockman[3], Mark Aronica[6], Kewal Asosingh[6], Donny D. Licatalosi[7], Jun Qin[8], Paul L. Fox[3], Thomas A. Hamilton[1], Donna Driscoll[3] and Xiaoxia Li[1]*

[1]Department of Immunology, Lerner Research Institute, Cleveland Clinic Foundation, Cleveland, OH, USA. [2]Department of General Biochemistry, Faculty of Biochemistry, Biophysics and Biotechnology, Jagiellonian University, Krakow, Poland. [3]Department of Cellular and Molecular Medicine, Lerner Research Institute, Cleveland Clinic Foundation, Cleveland, OH, USA. [4]Department of Immunology, Faculty of Biochemistry, Biophysics, and Biotechnology, Jagiellonian University, Krakow, Poland. [5]Department of Genetics, Stanford University School of Medicine, Stanford, California, USA. [6]Department of Pathobiology, Lerner Research Institute, Cleveland Clinic, Cleveland, OH, USA. [7]Center for RNA Molecular Biology, Department of Biochemistry, Case Comprehensive Cancer Center, Case Western Reserve University, Cleveland, OH, USA. [8]Department of Molecular Cardiology, Lerner Research Institute, Cleveland Clinic Foundation, Cleveland, OH, USA. [9]These authors contributed equally: Tomasz Herjan and Lingzi Hong. *e-mail: lix@ccf.org

© 2018 Nature America Inc., part of Springer Nature. All rights reserved.

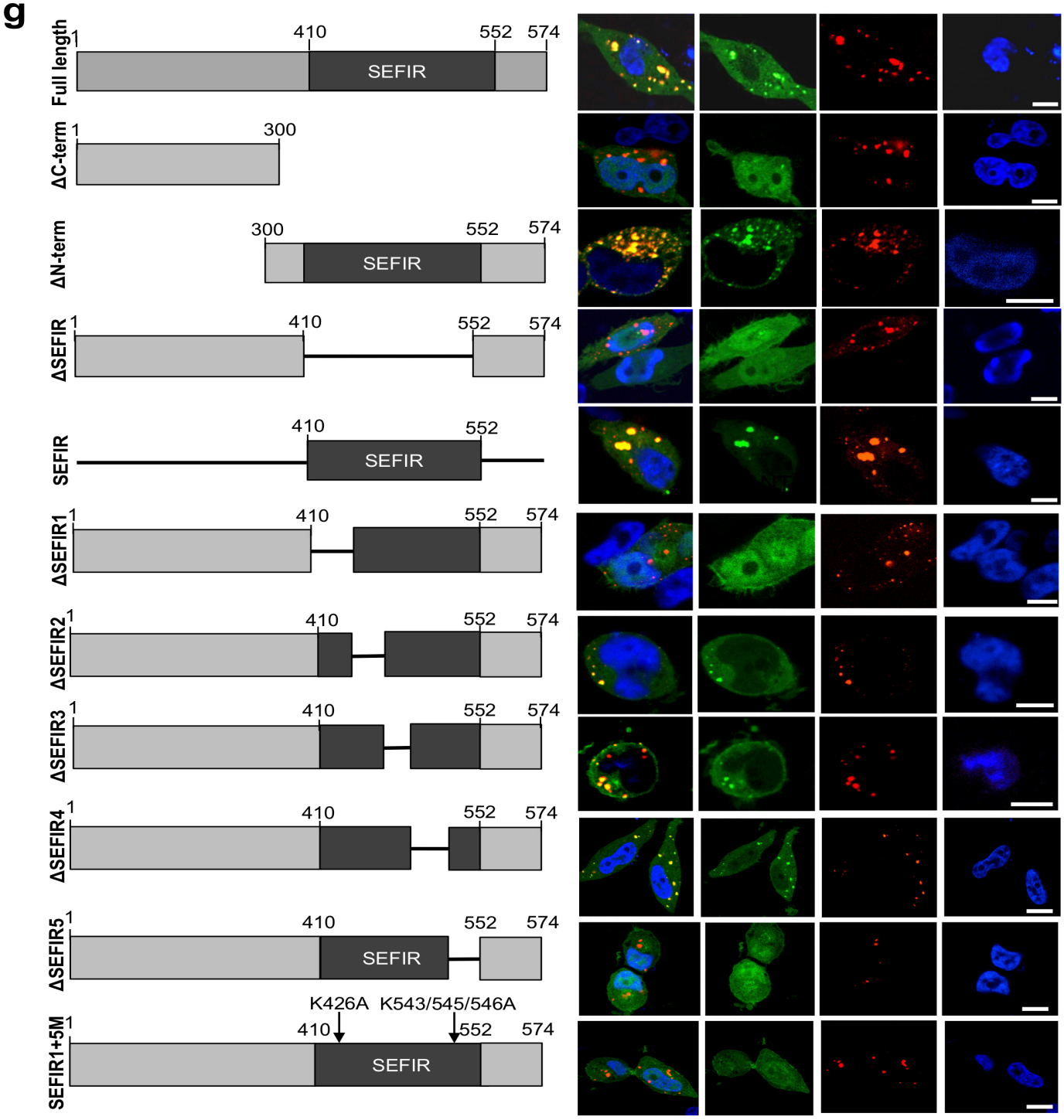


Supplementary Figure 1

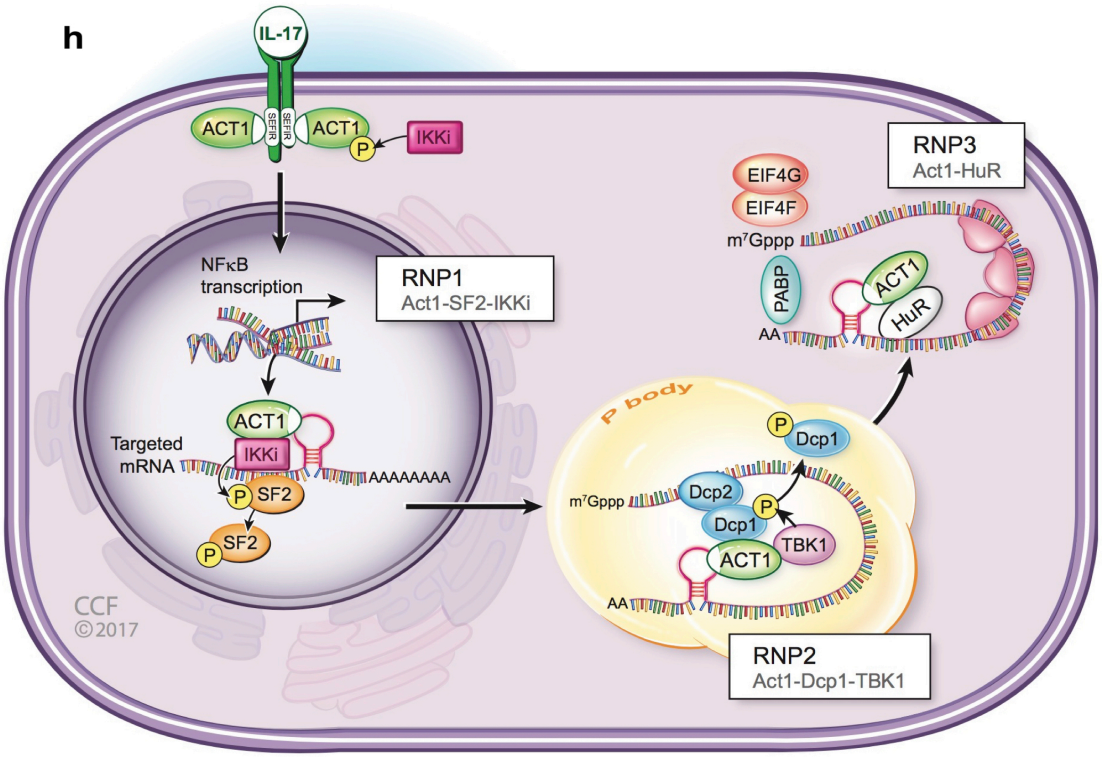


Supplementary Figure 1

.



Supplementary Figure 1

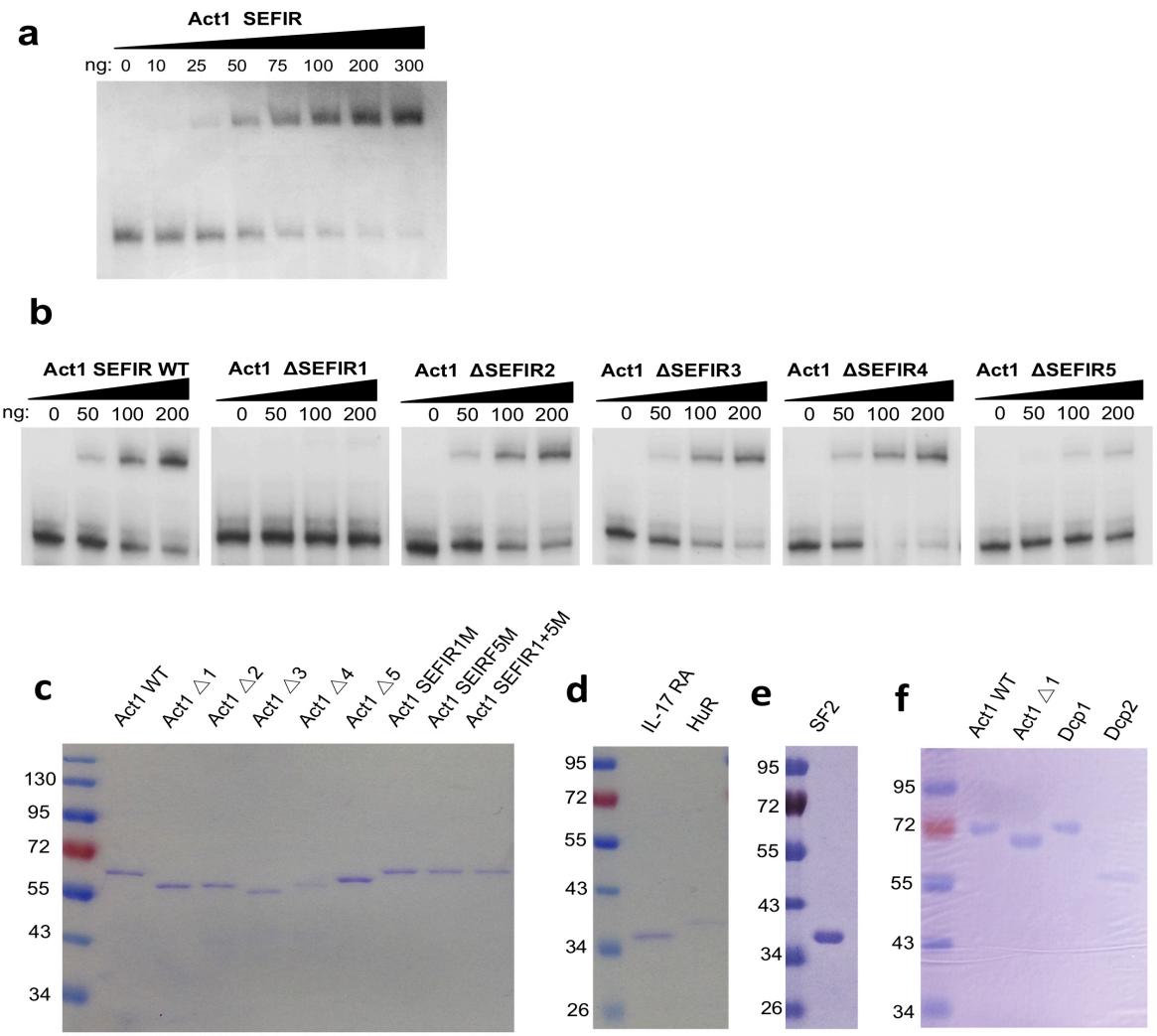


Supplementary Figure 1

IL-17A induces distinct Act1-RNPs in the nucleus and cytoplasmic granules.

a.MEFs isolated from LSL–HA–Act1 knock-in mice pre-treated with tamoxifen (10 ng/ml) for 72 hours were untreated or treated with IL-17A (50 ng/ml) for 1 hour, followed by confocal imaging of immunostaining with anti-HA (green HA-Act1) and anti-Dcp1 (red). Nuclei stained with DAPI in blue. The expression levels of the HA-Act1 were analyzed by western blotting. **b**. PLA in primary MEFs isolated from LSL–HA–Act1 knock-in mice, pre-treated with tamoxifen (10 ng/ml) for 72 hours and either left untreated or treated with IL-17A (50 ng/ml) for 1 hour and 24 hours. Anti-HA (rabbit) and Anti-Dcp1 (mouse) were used as primary antibodies followed by PLA probes. The red dots indicate the interaction of endogenous HA-Act1 and Dcp1. Nuclei stained with DAPI in blue. Bar graph shows the percentages of PLA positive cells with and without IL-17A stimulation. The quantification is based on the analysis of 50 cells with and without IL-17A stimulation. **c.** In situ PLA assay in MEFs isolated from LSL–HA–Act1 knock-in mice pre-treated with tamoxifen (10 ng/ml) for 72 hours and then untreated or treated with IL-17A (50 ng/ml) for 1 hour. Anti-HA (rabbit), anti-Dcp1 (mouse), anti-SF2 (mouse and rabbit) and anti-HuR (mouse and rabbit) were used. The red dots indicate the interaction of the two proteins as indicated. Nuclei stained with DAPI in blue. All bar graphs mean ± SD of three plates of cells. The exact P value for each comparison is provided on the graph or as p value < 0.001 . nd not detected. Cytoplasmic and nuclear fraction lysates from *Act1*$^{-/-}$ MEFs reconstituted by retroviral infection with either FLAG-tagged mouse wild-type Act1 (WT) or SEFIR1 deletion mutant stimulated with IL-17 (50 ng/ml) for the indicated time were lysed with or without RNase A and subsequently immunoprecipitated with anti-Dcp1a (**d)**, anti SF2 (**e**) and anti HuR (**f**) antibodies and analyzed by Western blot. The data shown were representative of three independent experiments. **g.** Confocal imaging of HeLa cells co-transfected with RPF-tagged Dcp1 and GFP-tagged Act1 constructs as indicated in the diagram (internal deletion mutants of the SEFIR domain are based on the five exons that encode regions of the SEFIR domain: 410 to 439, 440 to 462, 463 to 501, 502 to 526, and 527 to 552). Nuclei stained with DAPI in blue. The quantification of the data is shown in **fig. 1d.**

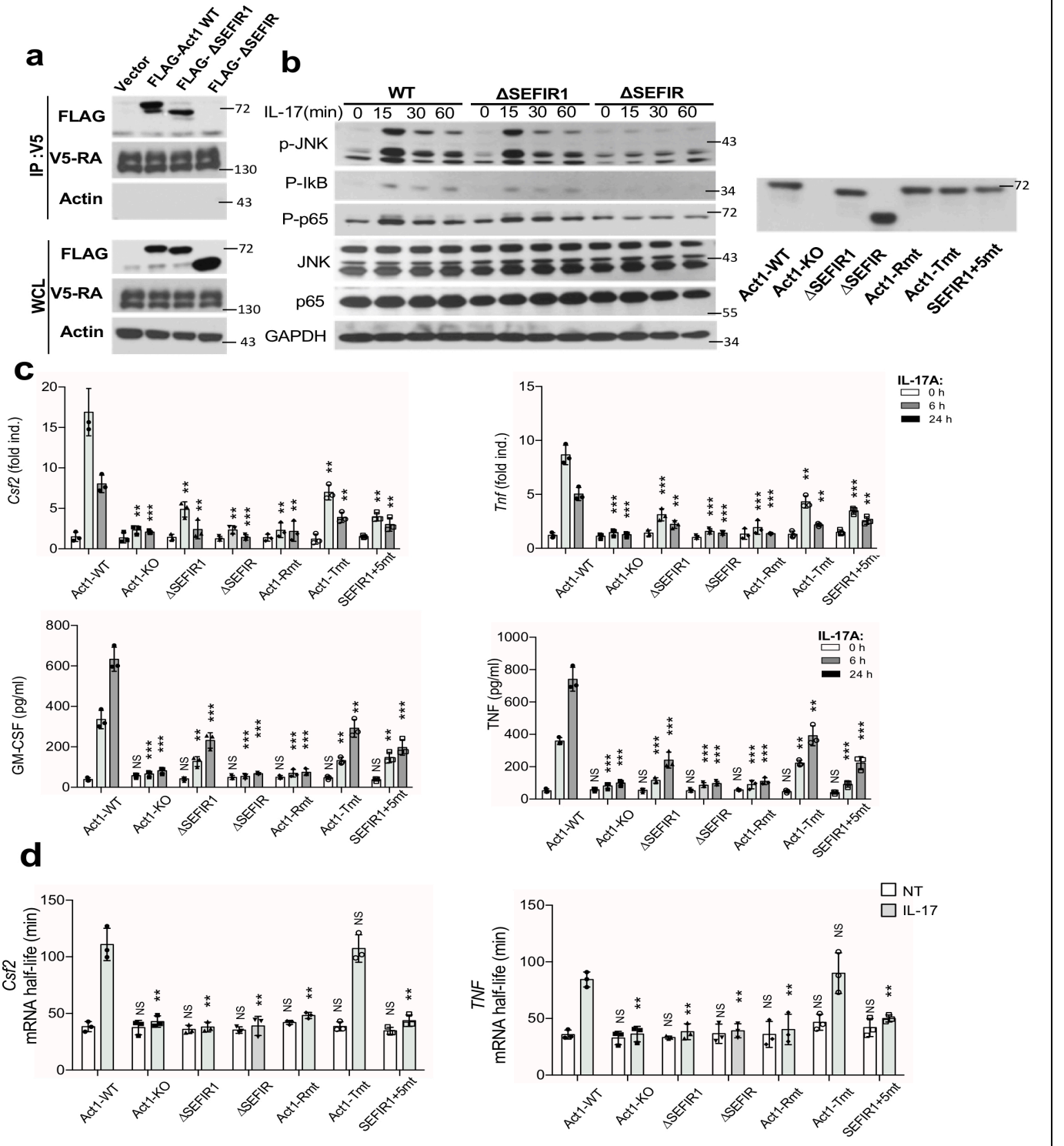
h. Model of Act1-RNP in mRNA stabilization: Act1 directly binds to the mRNAs of inflammatory genes to form multiple RNPs controlling different steps of mRNA metabolism in response to IL-17A stimulation. Upon IL-17A stimulation, Act1 is translocated into the nucleus where Act1 binds to a stem-loop structure in the 3'UTR in the target mRNAs (RNP1). The binding of Act1 competes off SF2 from the mRNAs by bringing IKKi to phosphorylate SF2, preventing SF2-mediated mRNA decay. Act1 then follows the mRNAs to the P-bodies (RNP2) inhibiting Dcp1/2-mediated mRNA decapping by employing TBK1 to phosphorylate Dcp1. Finally, Act1-mRNAs are shifted to the polysomes to facilitate HuR's binding to mRNAs (RNP3) for protein translation



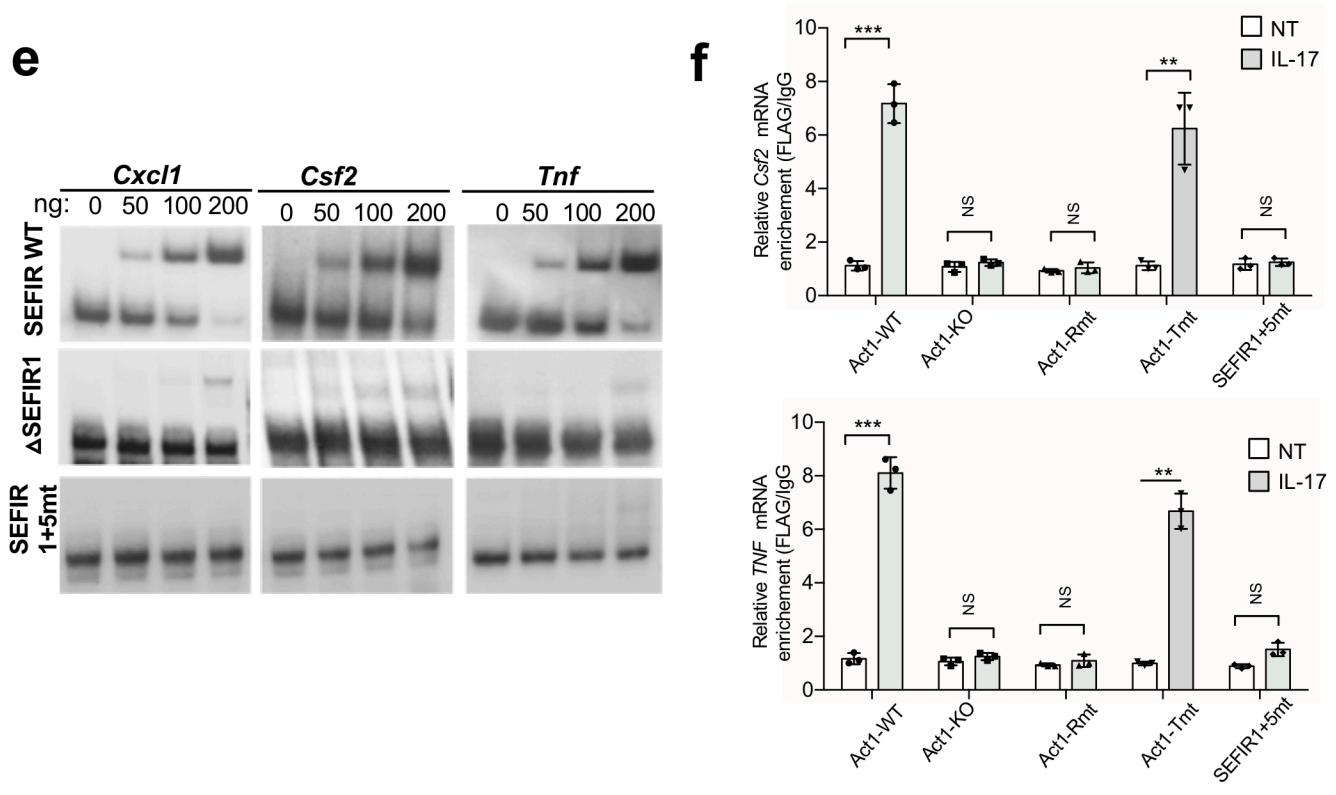
Supplementary Figure 2

Act1 directly binds to the CXCL1 3'UTR through the SEFIR domain

a. Binding of purified recombinant His-MBP-Act1 SEFIR to the *Cxcl1* 220 was examined *in vitro* by REMSA. Radiolabeled RNA probes were incubated with increasing amounts of protein as indicated. Free RNA was separated from RNA-protein complexes by native PAGE. The calculated apparent Kd of *Cxcl1* 220 for this experiment is shown in **Fig. 2b**. **b**. Binding of purified recombinant His-MBP-Act1 SEFIR and ΔSEFIR1, ΔSEFIR2, ΔSEFIR3, ΔSEFIR4 and ΔSEFIR5 to the *Cxcl1* 3'UTR (nt 720-940) by REMSA. **c-f.** Coomassie blue-stained SDS–polyacrylamide gel showing purified recombinant proteins including **(c)** Act1 SEFIR, SEFIR deletion mutants (ΔSEFIR1, ΔSEFIR2, ΔSEFIR3, ΔSEFIR4, ΔSEFIR5) and SEFIR point mutants (K407A; K524A/K526A/K527A; K407A/K524A/K526A/K527A)**; (d)** recombinant IL-17RA and HuR; **(e)** recombinant SF2. (**f**) Purified Act1 and Dcp1 proteins used for in vitro decapping assay.



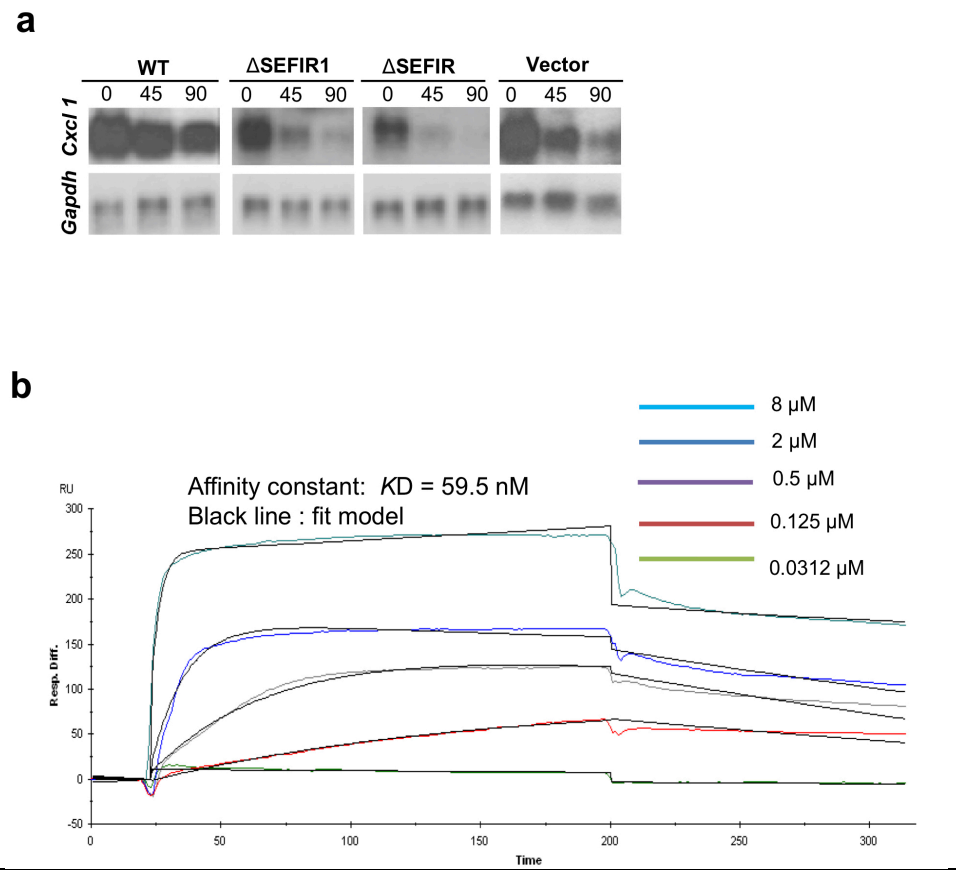
Supplementary Figure 3



Supplementary Figure 3

Act1 mediates mRNA stabilization of CXCL1, GM-CSF and TNF via direct binding to their 3'UTR

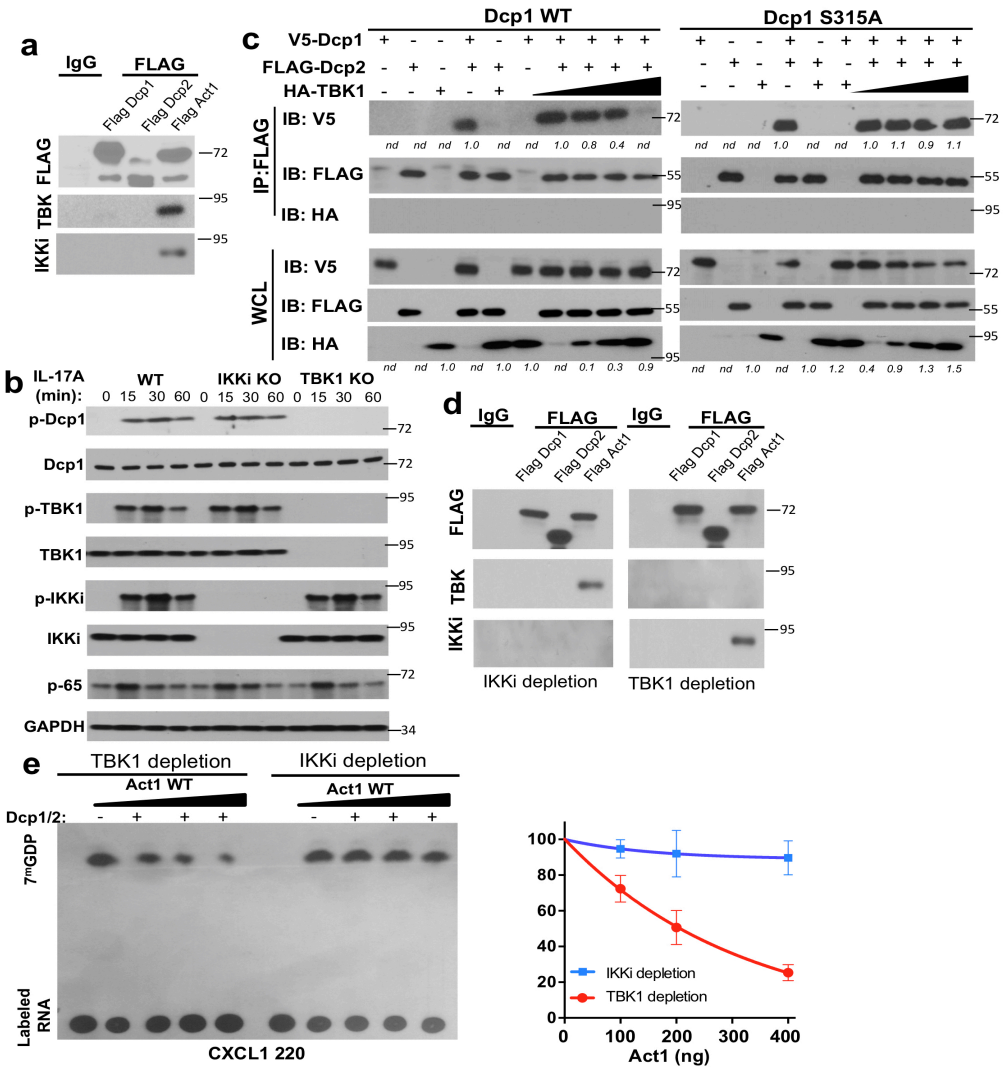
a.FLAG-tagged mouse Act1 or SEFIR deletion mutants were transfected into Hela cells with V5-tagged IL-17RA. The cell lysates of the transfected cells were immunoprecipated (IP) using anti-V5 followed by Western blot analyses using the indicated antibodies. Data are representative of two independent experiments. **b**. *Act1*$^{-/-}$ MEFs reconstituted by retroviral infection with either FLAG-tagged mouse wild-type Act1 (WT) or SEFIR deletion mutants were treated with IL-17A (50 ng/ml) for the indicated times. The expression levels of the transfected Act1 constructs in *Act1*$^{-/-}$ MEFs were analyzed by western blotting. The cell lysates were analyzed by Western blotting with the indicated antibodies. **c**. *Act1*$^{-/-}$ MEFs transfected with vector (Act1-KO), Act1 wild-type (Act1-WT) and Act1 mutants (DSEFIR1, DSEFIR, Act1-Rmt, Act1-Tmt and SEFIR1+5mt) pretreated with TNF (10 ng/ml) for 1 hour, either left untreated or stimulated with IL-17A (50 ng/ml) for 0, 6 or 24 hours. The mRNA and protein levels were analyzed by RT-PCR (Top) and Elisa (Bottom), respectively. Data are representative of two independent experiments (mean and s.d., Act1-WT versus Act1 mutants, by Student's t-test). **d**. *Act1*$^{-/-}$ MEFs transfected with vector (Act1-KO), Act1 wild-type (Act1-WT) and Act1 mutants (DSEFIR1, DSEFIR, Act1-Rmt, Act1-Tmt and SEFIR1+5mt) were pre-treated with TNF for 1 hour and then treated with Actinomycin D alone (NT) or in the presence of IL-17A (50 ng/ml) for 25, 50, 70, and 100min, followed by RT-PCR analysis (see Supple. Fig. 7I). The indicated mRNA levels were normalized to GAPDH and presented as half-life. Data are representative of two independent experiments (mean and s.d., Act1-WT versus Act1 mutants, by Student's t-test). **e**. Binding of purified recombinant His-MBP-Act1 SEFIR, DSEFIR1 and SEFIR1+5mt to the *Cxcl1* 3'UTR (720-940), *Tnf* 3'UTR (1362-1507) and *Csf2* 3'UTR (513-785) was examined by REMSA. **f**. *Act1*$^{-/-}$ MEFs transfected with vector (Act1-KO), flag-tagged Act1 wild-type (Act1-WT) and Act1 mutants (Act1-Rmt, Act1-Tmt and SEFIR1+5mt) were pre-treated with TNF (10 ng/ml) for 1 hour and then treated with IL-17A (50 ng/ml) for 0 and 60 min followed by RNA immunoprecipitation with anti-FLAG and RT-PCR analyses of the indicated mRNAs. The presented are the relative values to levels from IgG immunoprecipitation. Data are representative of two independent experiments All bar graphs show mean and s.d. of three separate plates of cells. The exact P value for each comparison is provided on the graph or as p value < 0.001 by two tailed Student's t-test.



Supplementary Figure 4

Act SEFIR binds and stabilizes *Cxcl1* mRNA

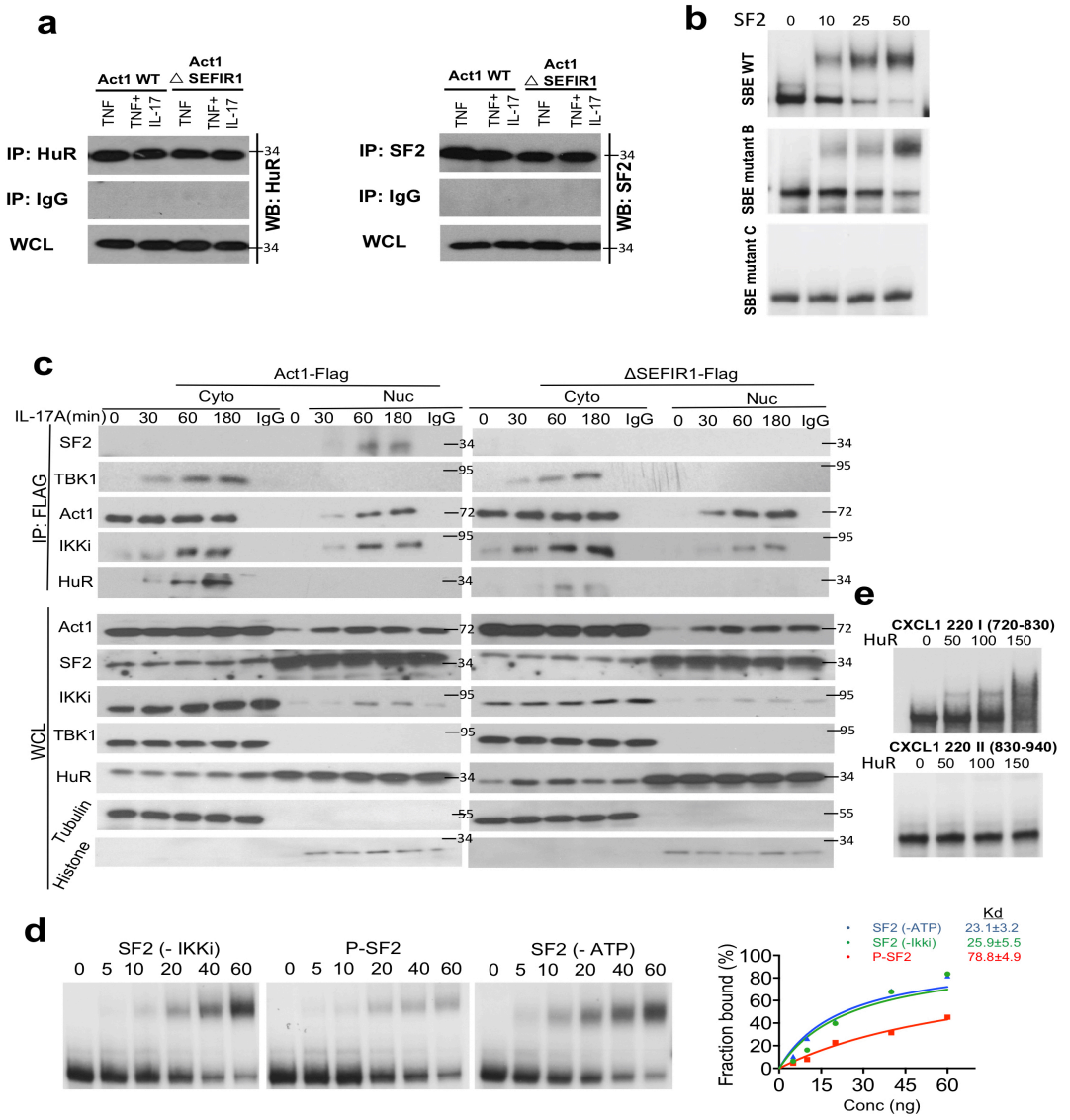
a.Wild-type Act1, SEFIR deletion mutants or empty vector were co-transfected into HeLa Tet-Off cells with pTRE2 (*Cxcl1* 220, nt 720-940, Datta et al., 2010), followed by treatment with doxycycline (detailed in Material and Methods). RNA samples were prepared from the transfected cells and subjected to RNA blot analysis. Graph indicates the *Cxcl1* mRNA levels normalized to *Gapdh* and presented as half-life. Data are representative of two independent experiments (mean and s.d., *, $p<0.05$ by Student's t-test). **b.** Act1 SEFIR-C *Cxcl1* SBE interaction was analyzed by SPR. Increasing concentrations of Act1 SEFIR (ranging from 31.2 nM to 8 µM) were passed over a sensor chip immobilized with *Cxcl1* SBE. Kinetic parameters were derived as described in 'Material and Methods' section.



Supplementary Figure 5

Act1-RNA binding to 3'UTR inhibits decapping through TBK1-mediated phosphorylation of Dcp1

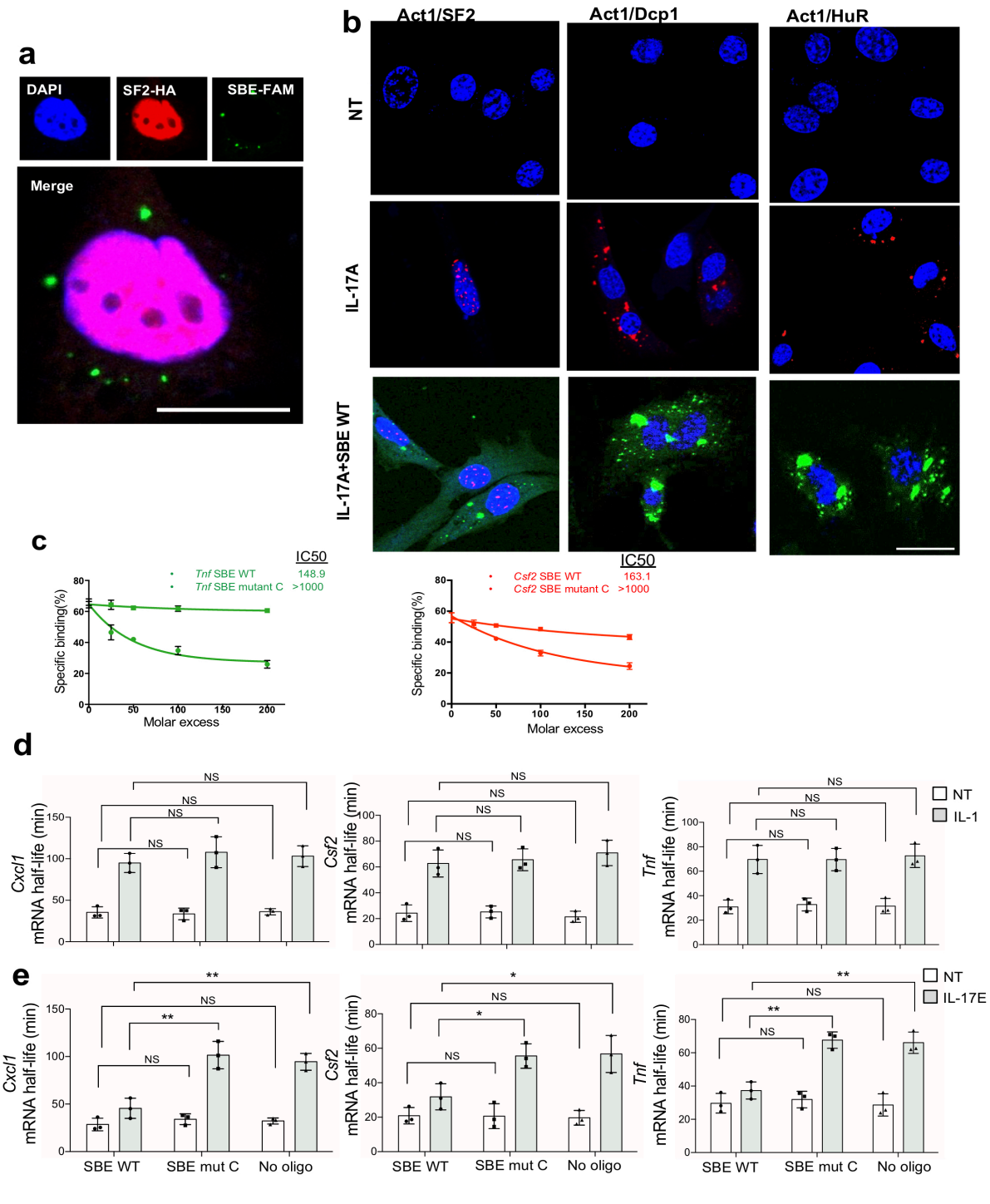
a.Lysates of HeLa cells transfected with FLAG-Dcp1, FLAG-Dcp2 or FLAG-Act1, were immunoprecipitated using beads conjugated with anti-FLAG and then eluted using 3 x FLAG peptide; eluates were analyzed by Western blot with anti-FLAG and anti-TBK antibody. **b.** Wild-type, IKKi-deficient (IKKi KO) and TBK1-deficient (TBK1 KO) MEFs were treated with or without IL-17A (50 ng/ml), followed by Western blot analysis using antibodies as indicated. Data are representative of two independent experiments. **c**. V5-tagged wild-type Dcp1 (left panel) or S315A mutant (right panel) were transfected into HeLa cells with HA-tagged TBK1 and/or FLAG-tagged Dcp2. The cell lysates were immunoprecipitated (IP) using anti-FLAG followed by Western blot analysis using the indicated antibodies. Data are representative of two independent experiments**.** Western blots were quantified by densitometry using ImageJ. **d**. Endogenous IKKi (left panel) or TBK1 (right panel) was immunodepleted using beads conjugated with anti-IKKi or anti-TBK1, respectively, from lysates of HeLa cells transfected with FLAG-Dcp1, FLAG-Dcp2 or FLAG-Act1. The supernatants (unbound lysates) after immunodepletion were immunoprecipitated using beads conjugated with anti-FLAG and then eluted using 3 x FLAG peptide; the eluates were analyzed by Western blotting with the indicated antibodies. **e**. Cap (m7GDP) labeled reporter *Cxcl1* **220** RNA was subjected to decapping assay using purified Dcp1/Dcp2 with increasing amounts of purified Act1 WT. Proteins were purified either from IKKi- or TBK1-immunodepleted lysates (as shown in **d,** and described in Materials and Methods). Graph indicates the decapping activity calculated by quantifying the released Cap as a percentage of the amount of Cap catalyzed by purified Dcp1/2. Data are representative of three independent experiments (mean and s.d.).



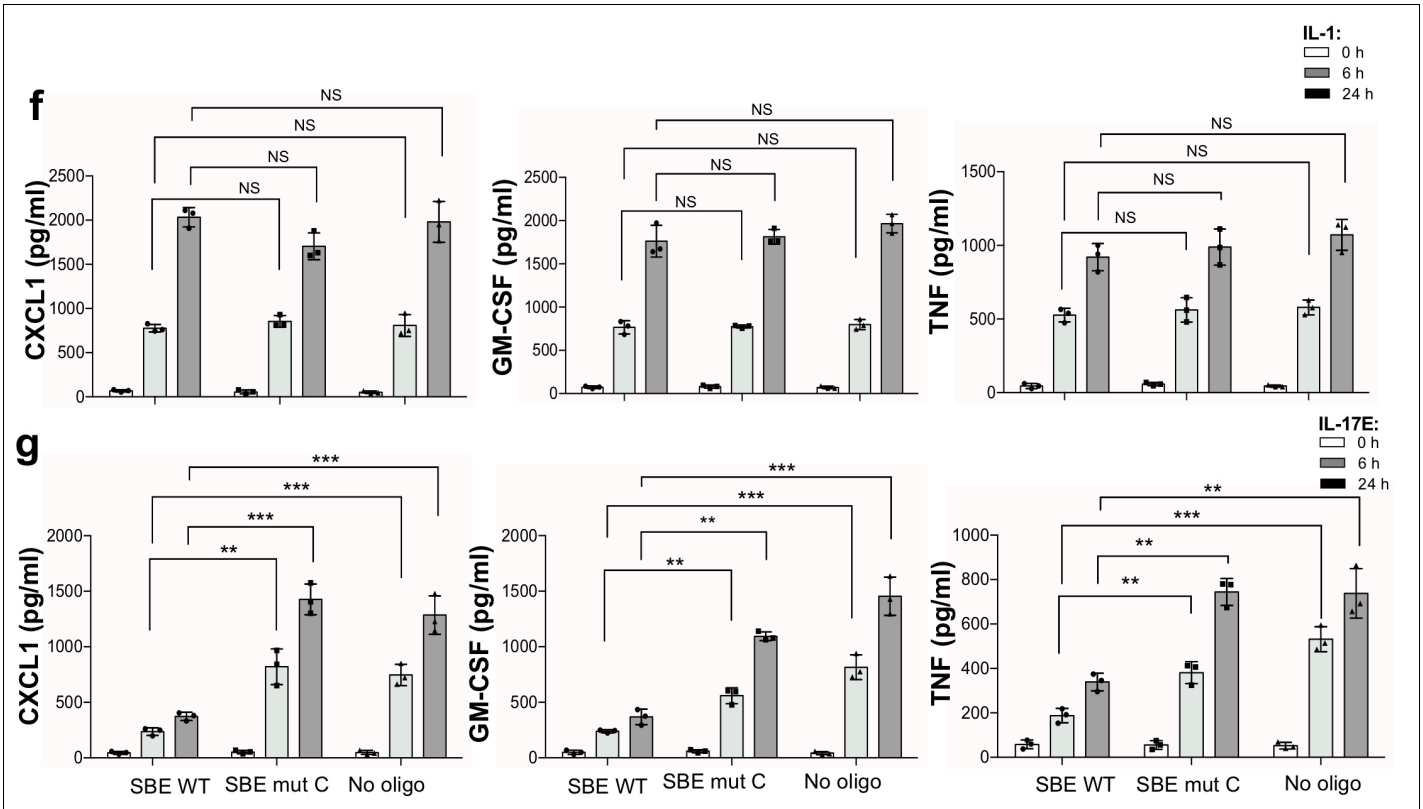
Supplementary Figure 6

Act1 forms distinct RNPs with Dcp1/Dcp2, SF2 and HuR in the nucleus and cytoplasm

a.*Act1*$^{-/-}$ MEFs reconstituted by retroviral infection with either FLAG-tagged mouse wild-type Act1 (WT) or SEFIR1 deletion mutant were pre-treated with TNF for 1 hour and then treated with IL-17 for 0 and 60 min followed by RNA immunoprecipitation with anti-SF2 or anti-HuR, followed by Western Blot analyses with the indicated antibodies. **b**. Binding of purified recombinant SF2 to SEFIR Binding Element (**SBE WT**, *Cxcl1* 47 as indicated in **Fig. 3a**) and stem-loop B and stem-loop C disruption mutants (**SBE mutant B** and **SBE mutant C**, Table 2 in Material and Methods) were examined by REMSA. **c**. Cytoplasmic and nuclear fraction lysates from *Act1*$^{-/-}$ MEFs reconstituted by retroviral infection with either FLAG-tagged mouse wild-type Act1 (WT) or SEFIR1 deletion mutant, stimulated with IL-17A (50 ng/ml) for the indicated times, were immunoprecipitated with anti-FLAG and analyzed by Western blots with the indicated antibodies. The experiments were repeated for two times. **d.** REMSA was performed to examine the binding of IKKi-phosphorylated SF2 (p-SF2) and non-phosphorylated SF2 (minus IKKi and minus ATP) to SEFIR Binding Element (SBE WT, *Cxcl1* 47 as indicated in **Fig. 3a**). Graph indicates the apparent Kd of *Cxcl1* 47, which was calculated as the concentration of SF2 protein required to achieve 50% binding of the RNA (Material and Methods). Data are representative of three independent experiments (mean and s.d.). **e**. Binding of purified recombinant HuR to *Cxcl1* 220-I (containing HuR binding site) and *Cxcl1* 220 II (containing SF2 and Act1 binding site) as indicated in **Fig. 5b** were examined by REMSA.



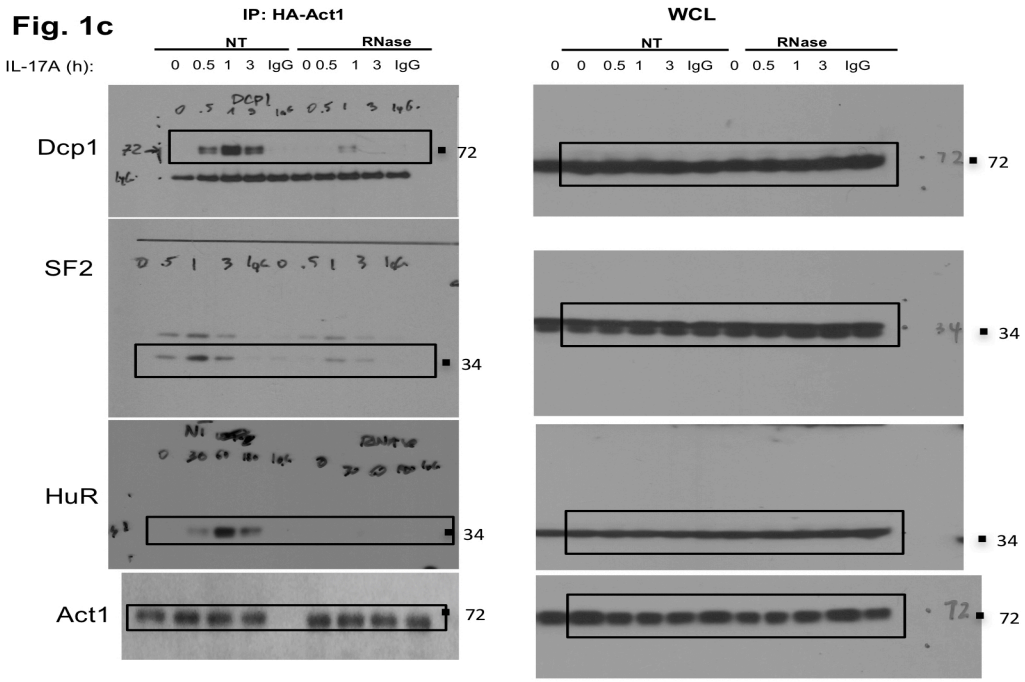
Supplementary Figure 7

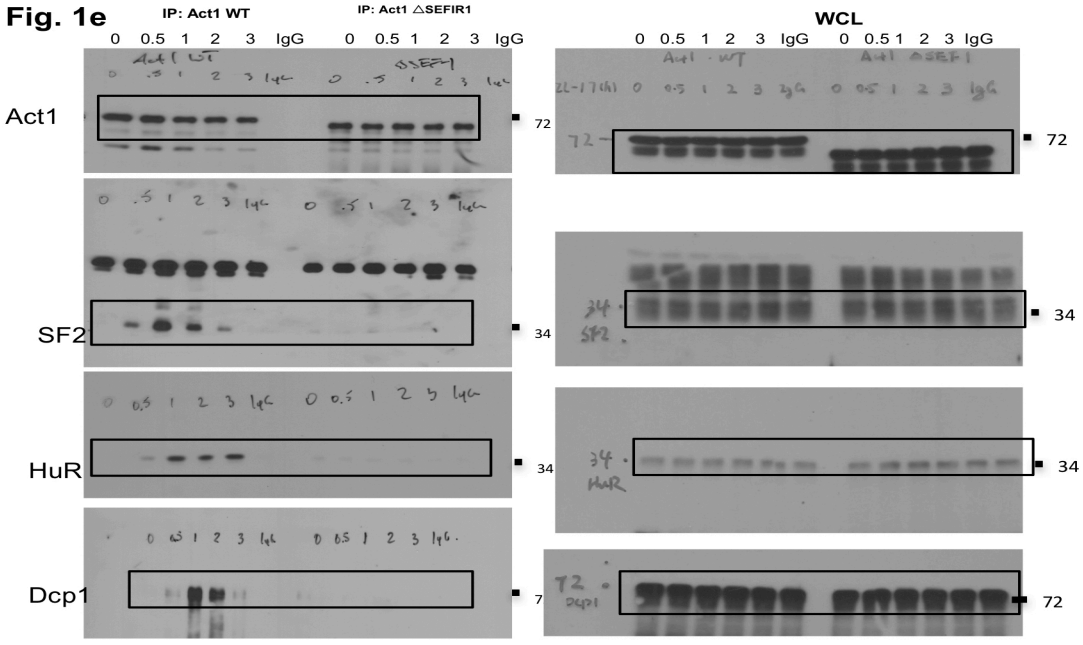


Supplementary Figure 7

SBE RNA aptamers abolished IL-17A and IL17E-induced mRNA stabilization of CXCL1, GM-CSF and TNF

a. Confocal imaging was used to analyze the localization of HA-SF2 and fluorescein amidite labeled SBE aptamer (SBE-FAM). HeLa cells were transfected with HA-SF2, followed by a second transfection with SBE-FAM 24hours later. Cells were fixed 20 hours after SBE-FAM transfection and subjected to immunofluorescent staining using anti-HA antibody. **b.** In situ PLA assay in MEFs isolated from LSL–HA–Act1 knock-in mice pre-treated with tamoxifen (10ng/ml) for 72 hours, followed by transfection with or without 100 pmoles/ml of SBE-FAM RNA aptamers (green). The transfected cells were untreated or treated with IL-17A (50 ng/m) for 1 hour. For PLA assay, anti-HA (rabbit), anti-Dcp1 (mouse), anti-SF2 (mouse) and anti-HuR (mouse) were used. The red dots indicate the interaction of HA-Act1 with SF2, Dcp1 or HuR. Nuclei stained with DAPI in blue. **c.** Graph quantifies the remaining Act1-SEFIR-bound *Csf2* or *Tnf* probe in the presence of indicated concentrations of SBE WT or SBE mutant C aptamers. IC50 is calculated as the concentration of aptamers that displace 50% of bound GM-CSF or TNF probe from the Act1-SEFIR. Data are representative of three independent experiments. Graph shows mean and s.d. of three separate plates of cells. **d** and **e** RNA decay in HeLa cells transfected with or without 100 pmoles/ml of SBE WT RNA aptamers, pre-treated with TNF (10 ng/ml) for 1 hour and then treated with Actinomycin D alone (NT) or in the presence of either IL-1 (10 ng/ml) or IL-17E (50 ng/ml) for 45 and 90 minutes. Human *Cxcl1, Csf2* and *Tnf* mRNAs were measured by RT-PCR, normalized to *Gapdh* and presented as half-life**.** Bar graph shows mean and s.d. of three separate plates of cells. Data are representative of three independent experiments. The exact P value for each comparison is provided on the graph or as p value < 0.001. **f-g.**HeLa cells transfected with or without 100 pmoles/ml of SBE RNA aptamers (WT or mutant C) were pre-treated with TNF (10 ng/ml) for 1 hour followed by stimulation with either IL-1 (10 ng/ml) or IL-17E (50 ng/ml) for 6 or 24 hours. Supernatants of the treated cells were then analyzed by ELISA. Data are representative of two independent experiments, analyzed by two-tailed Student's t-test. Bar graph represent mean ± SD of three independent plates of cells. The exact P value for each comparison is provided on the graph or as p value < 0.001.





Supplementary Figure 8

Fig. 2b

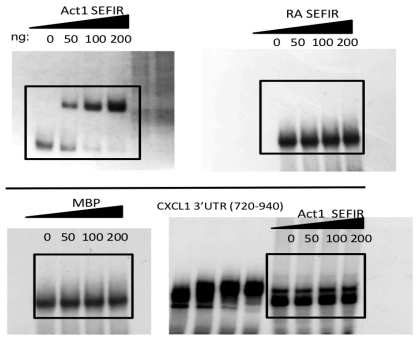


Fig. 2c

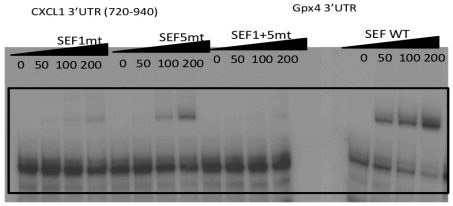


Fig. 2d

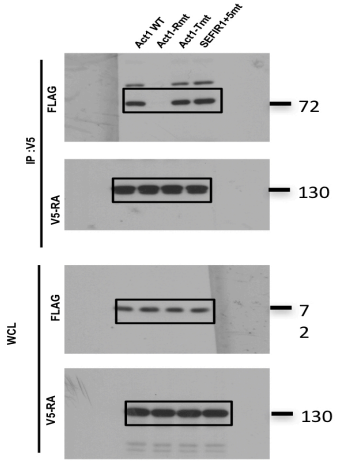
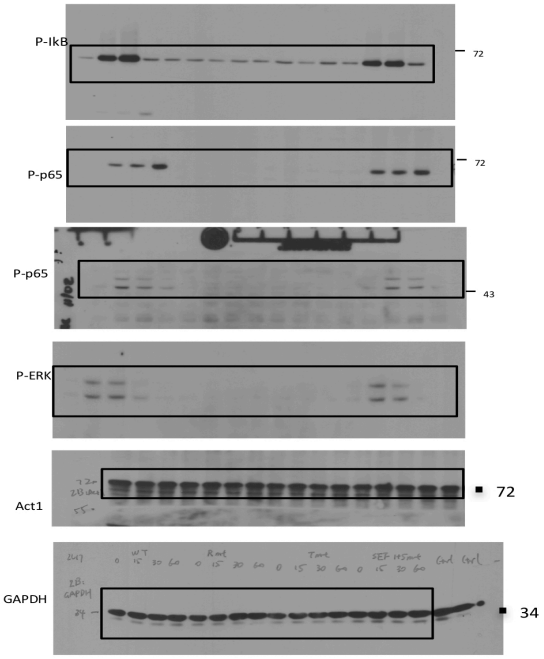


Fig. 2e



Supplementary Figure 8

Fig. 3b

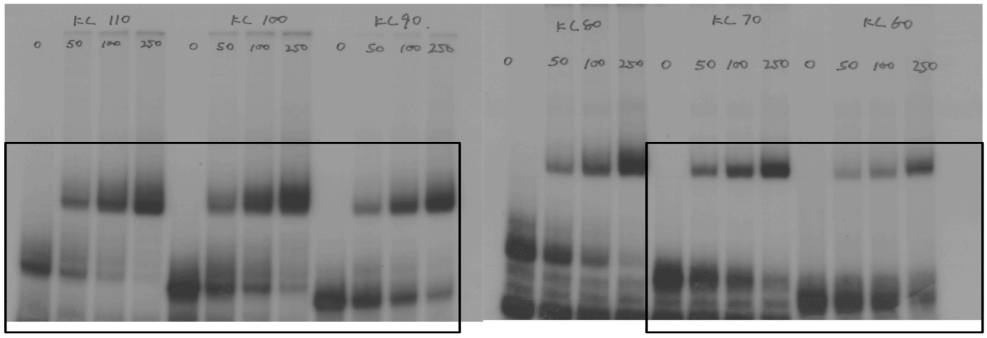


Fig. 3c

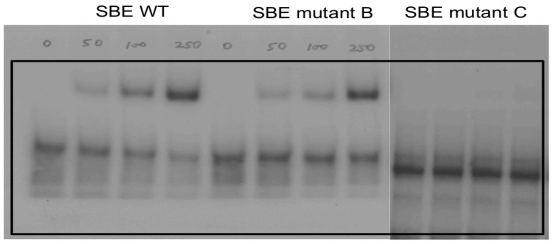


Fig. 3g

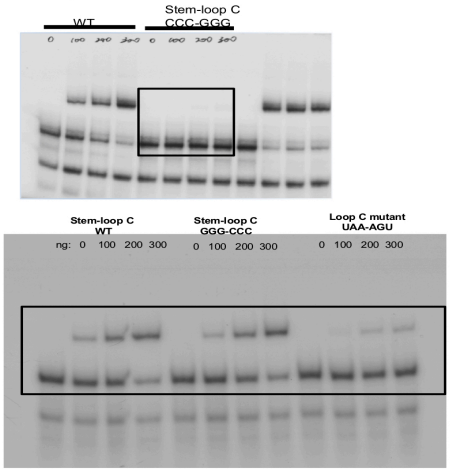
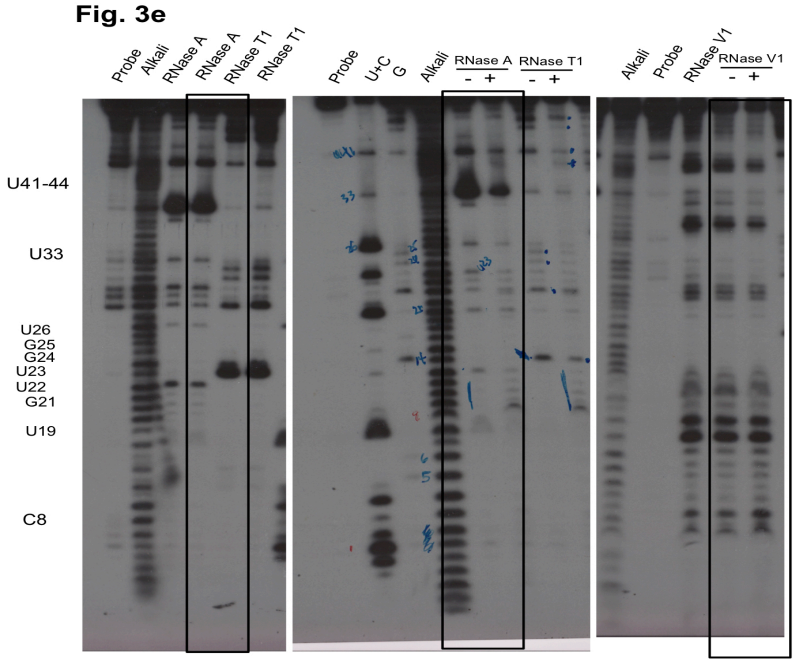
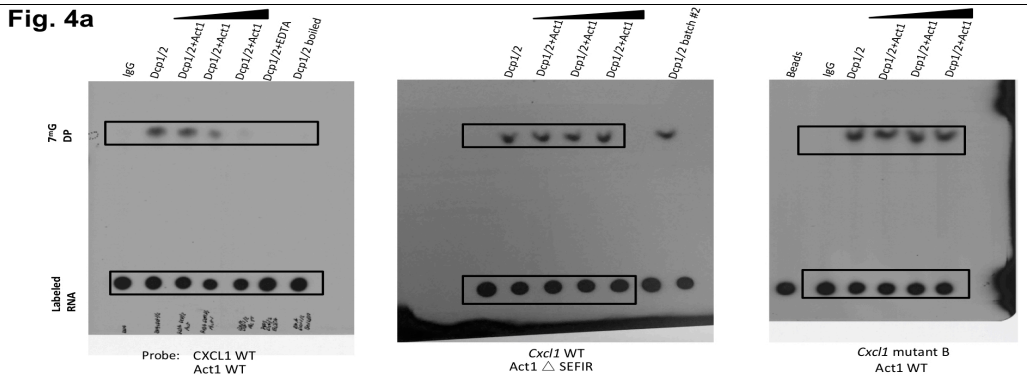
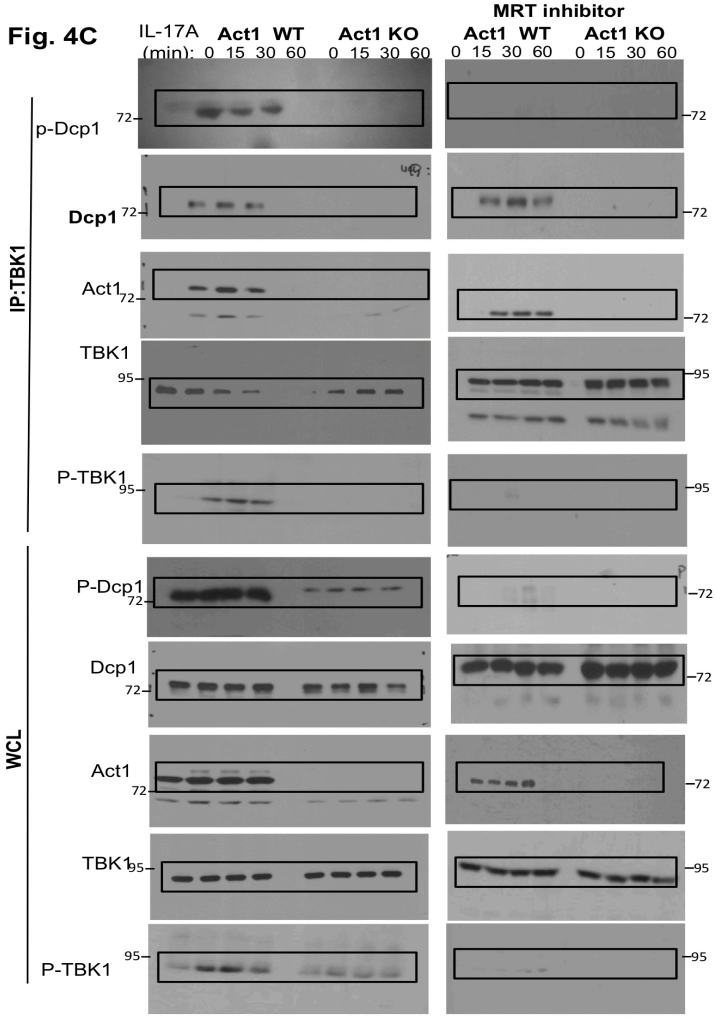


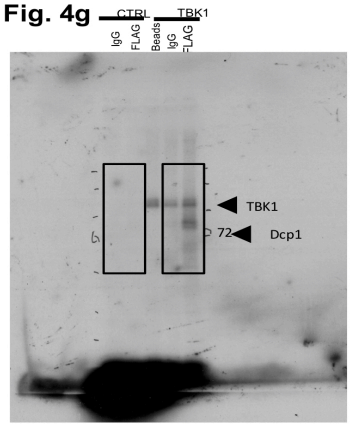
Fig. 3e

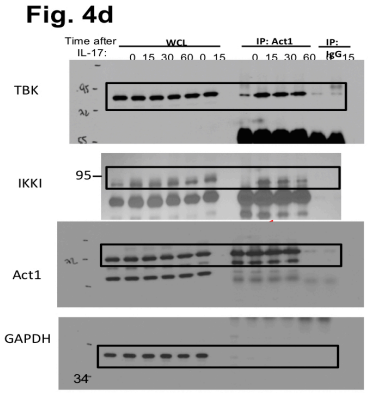


Supplementary Figure 8









Supplementary Figure 8

Fig. 5c

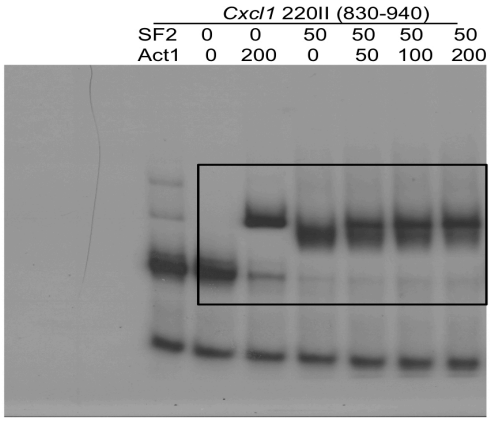


Fig. 5d

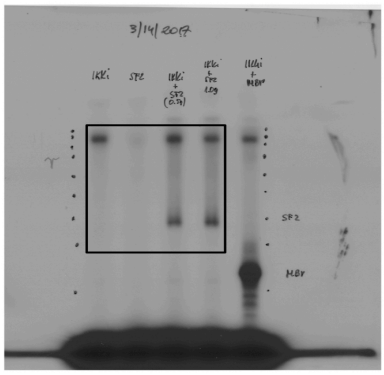


Fig. 5e

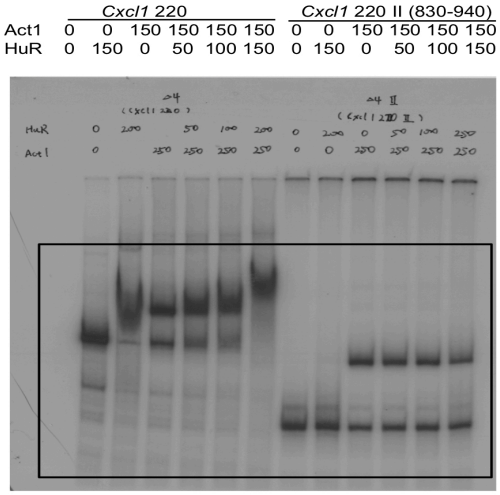
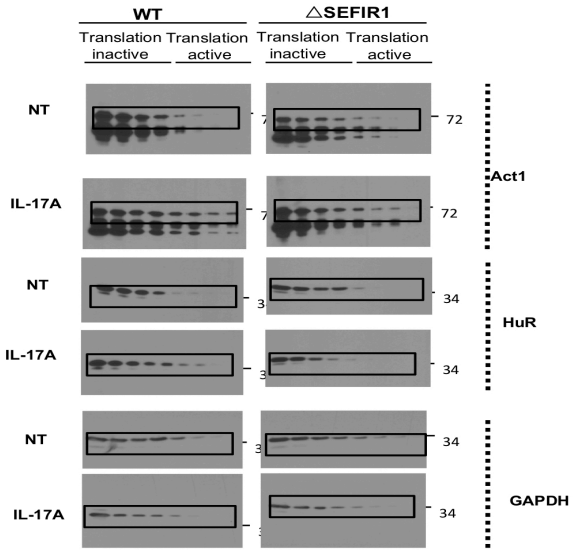


Fig. 5g



Supplementary Figure 8

Fig. 7a

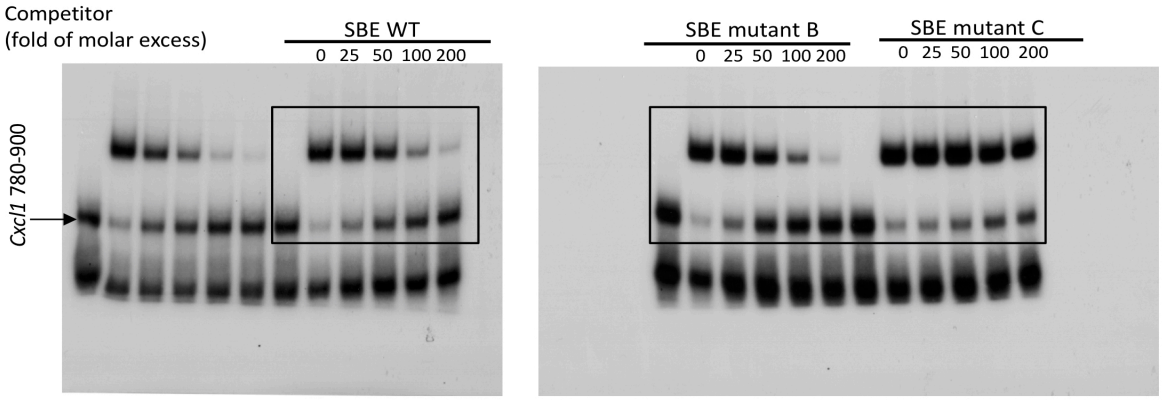
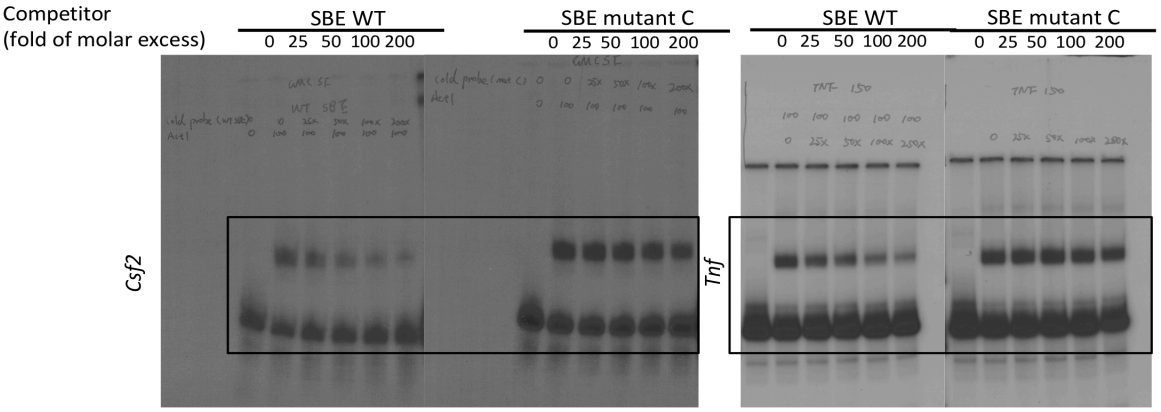


Fig. 7d



Supplementary Figure 8

Uncropped scans

Supplementary Table 1. Primers for real time quantitative PCR.

mCXCL1	F: CTGGCCACAGGGGCGCCTATC R: GGACACCTTTTAGCATCTTT
mCSF2	F: GGCCTTGGAAGCATGTAGAGG R: GGAGAACTCGTTAGAGACGACTT
mTNFα	F: CATCTTCTCAAAATTCGAGTGACAA R: TGGGAGTAGACAAGGTACAACCC
mGAPDH	F: GCCTTCCGTGTTCCTACCC R: TGCCTGCTTCACCACCTTC
mβ-actin	F: GGTCATCACTATTGGCAACG R: ACGGATGTCAACGTCACACT
hCXCL1	F: AACCGAAGTCATAGCCACAC R: GTTGGATTTGTCACTGTTCAGC
hCSF2	F: CACTGCTGCTGAGATGAATGAAA R: GTCTGTAGGCAGGTCGGCTC
hTNFα	F: TCAGCAAGGACAGCAGAG R: GTATGTGAGAGGAAGAGAACC
hβ-actin	F: GTCGGTATGGGTCAGAAAG R: CTCGTTGTAGAAGGTGTGG

Supplementary Table 2. Primers used for PCR

CXCL1 220	F: GGAAGAATTCCTGTGTTTGTATGTCTTG R: GGAAGGATCCCTTTTATTTTTACTTCATTT
CXCL1 120	F: GGAAGAATTCGTATGGTCAACACGCACGTGT R: GGAAGGATCCCTCTGTCCCGAGCGAGACG
CXCL1 110	F: ggaaGAATTCGTATGGTCAACACGCACGTG R: GGAAGGATCCCTCTGTCCCGAGCGAGACGAG
CXCL1 90	F: GGAAGGATCCCTCTGTCCCGAGCGAGACGAG R: GGAAGGATCCCTCTGTCCCGAGCGAGACGAG
CXCL1 80	F: GGAAGAATTCTTGACGCTTCCCTTGGAC R: GGAAGGATCCGACCAGGAGAAACAGGGTT
CXCL1 70	F: GGAAGGATCCGACCAGGAGAAACAGGGTT R: GGAAGGATCCACAGGGTTAAAGAATGTAAAAGGG
CXCL1 47	F: GGAAGAATTCCCTTGGACATTTTGTGTC R: GGAAGGATCCTGTAAAAGGGCATTATGCC
GPX1	F: CTGGTATCTGGGCTTGGTGATGG R: CTGGTATCTGGGCTTGGTGATGG
TNF 150	F:GGAAGGATCCTGTAAAAGGGCATTATGCC R:GGAAGGATCCGCTTATGTTTAAAACAAAATAT
GM-CSF	F:ggaaGAATTCgaccggccagatgaggctggcc R:GGAAGGATCCCTTGAATAAATATGGAATATG
hAct1-GFP	F:GGAAGCTAGCATGCCTCCTCAGCTTCAAG R:GGAAGTCGACTGCAAGGGAACCACCTGAAG
hDcp1a-GFP	F:GGAAGAATTCATGGAGGCGCTGAGTCGAGC R:GGAAGTCGACTGTAGGTTGTGGTTGTCTTTGTTC
hIKKi-GFP	F:GGAAGCTAGCATGCAGAGCACAGCCAATTAC R:GGAAGTCGACTGGACATCAGGAGGTGCTGGG
hTBK1-GFP	F:GGAAGGTACCATGCAGAGCACTTCTAATC

	R:GGAAGTCGACTGAAGACAGTCAACGTTGCG
hTIA-1-GFP	F:GGAAGCTAGCATGGAGGACGAGATGCCC R:GGAAGTCGACTGCTGGGTTTCATACCCTGCCAC
hAct1-RFP	F:GGAAGCTAGCATGCCTCCTCAGCTTCAAG R:GGAAGTCGACTGCAAGGGAACCACCTGAAG
hIRAK1-RFP	F:GGAAGCTAGCATGGCCGGGGGGCCGGGCCCG R:GGAAGTCGACTGGCTCTGAAATTCATCACTTTC
hDcp1a-RFP	F:GGAACTCGAGATGGAGGCGCTGAGTCGAGC R:GGAAGTCGACTGTAGGTTGTGGTTGTCTTTGTTC
V5-Dcp1a	F:GGAAGCTAGCGCCACCATGGATTACAAGGATGACGATGACAAGATG GAGGCGCTGAGTCGAGC R:GGAAGAATTCTCATAGGTTGTGGTTGTC
FLAG-hDcp1a	F:GGAAGCTAGCGCCACCATGGATTACAAGGATGACGATGACAAGATG GAGGCGCTGAGTCGAGC R:GGAAGAATTCTCATAGGTTGTGGTTGTC
FLAG-hDcp2	F:GGAAGCTAGCGCCACCATGGATTACAAGGATGACGATGACAAGATG GAGACCAAACGGGTGGAG R:GGAAGGATCCTCAAAGGTCCAAGATTTTC
FLAG-hIRAK1	F:GGAAGCTAGCGCCACCATGGATTACAAGGATGACGATGACAAGATG GCCGGGGGGCCGGGCCCG R: GGAAGAATTCTCAGCTCTGAAATTCATCACT
HA-hAct1	F: GGAAGCTAGCATGCCTCCTCAGCTTCAAG R: GGAAGAATTCTCACAAGGGAACCACCTGAAG

Supplementary Table 3. Selected REMSA probes

CXCL 220	cUgUgUUUgUaUgUcUUgaaaagaaUgUcagUUaUUUaUUgaaagUcgUcUU UcaUaUUgUaUggUcaacacgcacgUgUUgacgcUUcccUUggacaUUUUgUgU cUagUUggUagggcaUaaUgcccUUUUacaUUcUUUaacccUgUUUcUccUgg UcUcgUcUcgcUcgggacagagacgUUcaaaggacUgUUacaaaUgaagUaaaaaU aaaag
CXCL120	gUaUggUcaacacgcacgUgUUgacgcUUcccUUggacaUUUUgUgUcUagUUg gUagggcaUaaUgcccUUUUacaUUcUUUaacccUgUUUcUccUggUcUcgUc UcgcUcgggacagag
CXCL110	gUaUggUcaacacgcacgUgUUgacgcUUcccUUggacaUUUUgUgUcUagUUg gUagggcaUaaUgcccUUUUacaUUcUUUaacccUgUUUcUccUggUcUcgUc UcgcU
CXCL90	gUaUggUcaacacgcacgUgUUgacgcUUcccUUggacaUUUUgUgUcUagUUg gUagggcaUaaUgcccUUUUacaUUcUUUaacccUgUUUcUccUggUcUcgUc UcgcU
CXCL1 80	UUgacgcUUcccUUggacaUUUUgUgUcUagUUggUagggcaUaaUgcccUUU UacaUUcUUUaacccUgUUUcUccUggUc
CXCL1 70	UUgacgcUUcccUUggacaUUUUgUgUcUagUUggUagggcaUaaUgcccUUU UacaUUcUUUaacccUgUUUcUccUggUc

CXCL1 47 (SBE WU)	CcUUggacaUUUUgUgUcUagUUggUagggcaUaaUgcccUUUUaca
CXCL1 47 (SBE muUanUB)	CcUUggacaUUUUgUgUcUagUUggUagggcaUaaUgCCCUUUUaca
CXCL1 47 (SBE muUanUC)	CcUUggacaUUUUgUgUcUagUUggUaAAAcaUaaUgCCCUUUUaca
CXCL1 47 (SBE AGU)	CcUUggacaUUUUgUgUcUagUUggUagggcaAGUUgCCCUUUUaca
CXCL1 47 (SBE GGG-CCC swap)	CcUUggacaUUUUgUgUcUagUUggUaCCCcaUaaUgGGGUUUUaca
CXCL1 (SUem loop B)	UUgacgcUUcccUUggacaUUUUgUgUcUagUUggU
CXCL1 (SUem loop C)	gUUggUagggcaUaaUgcccUUUUac